Celestial Mechanics and Dynamical Astronomy manuscript No.
(will be inserted by the editor)

Describing relative motion near periodic orbits via local toroidal coordinates

Ian Elliott · Natasha Bosanac

Received: date / Accepted: date

Abstract Local toroidal coordinate systems are introduced to characterize relative motion near a periodic orbit with an oscillatory mode in the circular restricted three-body problem. These coordinate systems are derived from a first-order approximation of invariant tori relative to a periodic orbit and supply a geometric interpretation that is consistent across distinct periodic orbits. First, the local toroidal coordinate sets are used to rapidly generate first-order approximations of quasi-periodic relative motion. Then, geometric properties of these first-order approximations are used to predict the minimum and maximum separation distances between a spacecraft following quasi-periodic motion relative to another spacecraft located on a periodic orbit. Implementation of the local toroidal coordinate systems and associated geometric analyses are demonstrated in the context of spacecraft formations operating near members of the Earth-Moon L_2 southern halo orbit family.

Keywords Relative motion · Quasi-periodic orbits · Toroidal coordinates · Circular restricted three-body problem

1 Introduction

Missions that involve spacecraft operating in multi-body gravitational environments and beyond the primary gravitational influence of the Earth have been of increasing interest for scientific, technological, and exploration purposes. For instance, space telescopes have been and will continue to operate near the libration points in the Sun-Earth system (Burt and Smith 2012; Gardner et al. 2009; Spergel et al. 2015). In-space assembly within the Earth-Moon and Sun-Earth systems has also been identified as a key technology for new scientific missions and extending the lifetime of space assets (Belvin et al. 2016). Notably, NASA's Artemis program

I. Elliott
Graduate Researcher, Colorado Center for Astrodynamics Research, Smead Department of Aerospace Engineering Sciences, University of Colorado Boulder, 429 UCB, 3775 Discovery Drive, Boulder CO, 80303
E-mail: ian.elliott@colorado.edu

N. Bosanac
Assistant Professor, Colorado Center for Astrodynamics Research, Smead Department of Aerospace Engineering Sciences, University of Colorado Boulder, 429 UCB, 3775 Discovery Drive, Boulder CO, 80303
E-mail: natasha.bosanac@colorado.edu

includes the near-future in-space assembly of Gateway, a space station that is currently expected to closely follow an Earth-Moon L_2 near-rectilinear halo orbit (Crusan et al. 2018). Future constellations of spacecraft may also operate in multi-body systems as space-based interferometers (Kasper et al. 2019). When designing trajectories for these applications, spacecraft often follow bounded trajectories resembling periodic orbits that exist in a low-fidelity dynamical model labeled the Circular Restricted Three-Body Problem (CR3BP) (Dunham and Roberts 2001). Additional assets such as servicing modules, components, or starshades may rendezvous with or maintain a desired path relative to the primary spacecraft (Farres et al. 2018; Le Moigne 2018). In these scenarios, generalized and geometrically-interpretable insight into the characteristics of relative motion between spacecraft in complex, multi-body gravitational systems is necessary to support the development of proximity operation guidelines and formation flying guidance and control schemes.

Spacecraft formations have been operating near circular (Clohessy and Wiltshire 1960) and elliptical orbits (Sengupta and Vadali 2007; Tschauner and Hempel 1965) near the Earth for decades. In this regime, the relative motion between two spacecraft is well-understood using equations of relative motion expressed in a local coordinate system defined by the target spacecraft (Alfriend et al. 2009). Relative orbital element sets and geometry-based coordinate sets may also be used to introduce geometric insight into the description of spacecraft relative motion in two-body systems (Bennett and Schaub 2016; Schaub and Junkins 2014). For instance, Keplerian orbital element differences between spacecraft within a formation admit relative state representations that vary slowly with time in perturbed two-body environments (Schaub 2004). These slowly-varying state descriptions are useful for formation flying control schemes and have been successfully applied in the guidance and control of previous spacecraft missions (Gill et al. 2007; Montenbruck et al. 2008). Carter (1998) and Sullivan et al. (2017) also present comprehensive surveys of spacecraft relative motion dynamics models, including orbital element difference models, to capture the state-of-the-art of spacecraft relative motion models in predominantly two-body environments.

Relative motion in multi-body systems is significantly more complex to examine than in Keplerian regimes due to the chaotic nature of the underlying solution space; as a result, there is currently limited heuristic insight into relative motion in multi-body systems. Investigations into the impact of third-body gravitational perturbations on spacecraft formations have been examined via conic-based differential orbital elements (Roscoe et al. 2013) and hybrid orbital element systems (Bakhtiari et al. 2017). However, as general trajectories in multi-body systems are not well-approximated by conics, they are often analyzed in a rotating frame defined by two celestial bodies using approximated dynamical models such as the CR3BP (Gurfil and Kasdin 2004). One approach to studying relative motion in the CR3BP begins with constructing nonlinear and linearized equations of relative motion formulated in a local-vertical, local-horizontal frame, such as those recently presented by Franzini and Innocenti (2019). Additional studies have focused on identifying spacecraft formation configurations that exhibit low natural relative drift relative to a periodic orbit in the CR3BP (Ferrari and Lavagna 2018; Héritier and Howell 2014). However, the sensitivity and variety of the solution space for relative trajectory design still presents challenges for the extraction of meaningful heuristics. This paper seeks to contribute to addressing the challenges by describing relative motion near periodic orbits and leveraging insight gained via dynamical systems theory.

Thorough analyses of the CR3BP and the solution space admitted by this autonomous dynamical model have been conducted in the astrodynamics community (Koon et al. 2006; Szebehely 1967). The CR3BP admits several fundamental solutions, including five equilibrium points, and infinite families of periodic and quasi-periodic orbits. Periodic orbits near libration points have been identified as advantageous locations for long-term placement of single spacecraft in multi-body environments in early studies by Farquhar (1971), Breakwell and Brown (1979), and Howell (1984). Furthermore, quasi-periodic orbits, which naturally trace invariant tori that envelope a nearby periodic orbit, have been identified as a useful reference for natural formations of spacecraft in multi-body environments (Barden and Howell 1998b; Gómez et al. 1998; Lo 1999). Early investigations by Barden and Howell (1998a,b) and Gómez et al. (1998) demonstrate that spacecraft following quasi-periodic orbits in the CR3BP remain naturally bounded and exhibit quasi-periodic motion relative to an associated periodic orbit. Building upon these works, additional investigations into relative trajectory design have used invariant tori in a variety of nonlinear gravitational models and scenarios (Baresi and Scheeres 2017; Baresi et al. 2016; Henry and Scheeres 2021; McCarthy and Howell 2021). Furthermore, quasi-periodic trajectories have been identified and examined as a useful reference for spacecraft formation control (Howell and Marchand 2005).

As demonstrated by Gómez et al. (1998), Kolemen et al. (2012) and Olikara and Scheeres (2012), the computation of quasi-periodic orbits in the nonlinear CR3BP is an expensive numerical process. Analyzing first-order approximations of invariant tori relative to periodic orbits in the CR3BP, Howell and Marchand (2005) determine that they supply sufficient representations of solutions that exist in the local neighborhood of a periodic orbit in the nonlinear CR3BP, as well as in higher fidelity ephemeris models. Additionally, using insight from Kolmogorov–Arnold–Moser (KAM) theory, Barden and Howell (1999) demonstrate that first-order approximations of invariant tori relative to periodic orbits in the CR3BP may be captured in point-mass ephemeris models with conservative perturbations. These results motivate leveraging approximations of quasi-periodic motion as computationally-inexpensive mechanisms for studying bounded relative motion for formation flying near periodic orbits in multi-body systems.

Quasi-periodic motions possess complex, time-varying descriptions relative to periodic orbits when expressed using Cartesian coordinates. In Hamiltonian systems, action-angle coordinates are a fundamental method for describing states that lie on the surface of a torus (Meiss 2007). However, in multi-body gravitational environments, numerically computing these coordinates via normal form expansions tends to be computationally intensive (Jorba and Masdemont 1999). Alternatively, Floquet analysis of periodic orbits in the CR3BP, as analyzed by Wiesel and Shelton (1983), Simó et al. (1987), and Barden and Howell (1998b), enables decomposition of the state of a spacecraft relative to a periodic orbit, regardless of the stability, using the Floquet modes of the orbit. Because Floquet modes are periodic, and do not exponentially grow or decay over time, using Floquet modes as a basis introduces insight into the state of a spacecraft relative to a periodic orbit as a combination of the associated eigenspaces (Calico and Wiesel 1984). Additionally, Hsiao and Scheeres (2002) introduce a set of linearized relative orbital elements to describe oscillatory motion stabilized relative to a periodic orbit via feedback control formulated using eigenspace information, producing solutions with similar characteristics to motion within a natural center eigenspace (Scheeres et al. 2003). The current work in this paper builds upon these approaches that incorporate information about the local eigenspaces of a periodic orbit, via eigendecomposition or Floquet mode analysis.

In this paper, local toroidal coordinate systems are introduced to describe motion relative to a periodic orbit with oscillatory modes in the CR3BP. The presented coordinate systems leverage the geometric characteristics of a nearby invariant 2-torus and are applicable to periodic orbits in the CR3BP that possess at least one oscillatory mode, regardless of the overall stability of the orbit. First, nonlinear and linear equations of relative motion are presented, assuming that the dynamics of each spacecraft are modeled via the CR3BP. Then, the procedure for calculating a first-order approximation of an invariant 2-torus in the linearized equations of relative motion is summarized. This fundamental structure is used as a reference for defining the two local coordinate systems for periodic orbits: a nonsingular set and a geometrically-defined set. Mappings between Cartesian states, defined in the rotating frame of the CR3BP and relative to a periodic orbit, and the local toroidal coordinates and coordinate rates are presented. In both of these local toroidal coordinate systems, first-order approximations of invariant 2-tori exist as equilibrium solutions to the linearized equations of relative motion. The local toroidal coordinates, combined with insight into the geometric structure of the first-order approximation of an invariant 2-torus, also facilitate rapid prediction of the minimum and maximum possible separation between a spacecraft located along an approximated 2-torus and another spacecraft located on the periodic orbit; information that is useful in applications such as formation design, proximity operations, and safe trajectory design for rendezvous and docking. Implementation of the introduced local toroidal coordinate systems is demonstrated in the context of relative motion near various members of the Earth-Moon southern L_2 halo orbit family in the CR3BP. This analysis includes examining the errors associated with the coordinate set description and predicting the separation envelopes of quasi-periodic relative motion.

2 The circular restricted three-body problem

The CR3BP is employed to model the natural motion of a spacecraft in a multi-body system. In this dynamical model, a spacecraft is assumed to be influenced by point-mass gravitational interactions with two constant mass primary bodies (Szebehely 1967); in this paper, the Earth and Moon. These two primaries, labeled as P_1 and P_2, are assumed to follow circular orbits about their mutual barycenter. The two primaries are labeled with P_1 possessing a mass m_1 that is greater than or equal to m_2, the mass of P_2. The mass of the spacecraft, P_3, and its gravitational effect on the two primary bodies are assumed to be negligible. A nondimensionalization scheme is also often employed: length quantities are normalized by the distance between the two primary bodies, time quantities are normalized such that the mean motion of the two primaries about their barycenter is equal to unity, and mass quantities are normalized using the total mass of the system (Szebehely 1967). A system mass ratio, μ, is then defined as $\mu = m_2/(m_1 + m_2)$ (Szebehely 1967); in the Earth-Moon CR3BP, $\mu \approx 0.01215$. This nondimensionalization scheme facilitates extrapolation between systems with similar mass ratios and to reduce the potential for ill-conditioning in numerical integration. However, dimensional quantities are used for reporting results in this paper.

To describe the state of a spacecraft in the CR3BP, two coordinate frames are defined: an inertial frame and a rotating frame. The rotating frame, $\mathcal{R}$, is defined with axes $\{\hat{\boldsymbol{x}}, \hat{\boldsymbol{y}}, \hat{\boldsymbol{z}}\}$: $\hat{\boldsymbol{x}}$ is directed from P_1 to P_2, $\hat{\boldsymbol{z}}$ is parallel to the orbital angular momentum vector of the primary system, $\boldsymbol{h}$, and $\hat{\boldsymbol{y}}$ completes the right-handed triad. Next, an inertial frame, $\mathcal{N}$, is defined using axes $\{\hat{\boldsymbol{X}}, \hat{\boldsymbol{Y}}, \hat{\boldsymbol{Z}}\}$. The third axis of the rotating frame $\hat{\boldsymbol{z}}$ is always aligned with the third axis of the inertial frame, $\hat{\boldsymbol{Z}}$. Accordingly, the transformation from the inertial to the rotating frame is a counter-clockwise rotation about $\hat{\boldsymbol{Z}}$. Under the assumption that the primary bodies follow circular orbits, the nondimensional angular velocity vector of the rotating frame with respect to the inertial reference frame is $\boldsymbol{\omega}_{RN} = 1\hat{\boldsymbol{z}}$.

The equations of motion for the CR3BP are formulated relative to the system barycenter and in the rotating frame. First, the nondimensional state vector of the spacecraft relative to the system barycenter is defined in the rotating frame as $\boldsymbol{x} = [x, y, z, \dot{x}, \dot{y}, \dot{z}]^T$. The first three components of this vector form the position vector of the spacecraft, denoted as $\boldsymbol{r}_3 = [x, y, z]^T$. The equations of motion for a spacecraft in the CR3BP are then written using the nondimensional acceleration of the spacecraft with respect to the system barycenter, formulated in the rotating frame as

$$\boldsymbol{r}_3'' = \ddot{\boldsymbol{r}}_3 - 2\left(\boldsymbol{\omega}_{RN} \times \boldsymbol{r}_3'\right) - \boldsymbol{\omega}_{RN} \times (\boldsymbol{\omega}_{RN} \times \boldsymbol{r}_3) \tag{1}$$

where $(\ )'$ indicates a time derivative of a vector for an observer fixed in the rotating frame and $(\dot{\ })$ indicates a time derivative of a vector for an observer fixed in the inertial frame. In addition, the time derivative of a scalar quantity is indicated using the $(\dot{\ })$ notation for brevity. In this expression, the nondimensional inertial acceleration of the spacecraft in the CR3BP is equal to (Vallado and McClain 2013)

$$\ddot{\boldsymbol{r}}_3 = -(1-\mu)\frac{\boldsymbol{r}_{13}}{r_{13}^3} - \mu\frac{\boldsymbol{r}_{23}}{r_{23}^3} \tag{2}$$

where r_{13} and r_{23} are the distances of the spacecraft from P_1 and P_2, respectively. To calculate these quantities, note that the position vectors of the two primary bodies are equal to $\boldsymbol{r}_1 = -\mu\hat{\boldsymbol{x}}$ and $\boldsymbol{r}_2 = (1-\mu)\hat{\boldsymbol{x}}$ in the rotating frame and relative to the barycenter. Finally, the equations of motion of the CR3BP are commonly expressed as

$$\ddot{x} = 2\dot{y} + \frac{\partial U^*}{\partial x}, \qquad \ddot{y} = -2\dot{x} + \frac{\partial U^*}{\partial y}, \qquad \ddot{z} = \frac{\partial U^*}{\partial z} \tag{3}$$

where U^* is a pseudo-potential function, defined as (Breakwell and Brown 1979)

$$U^* = \frac{x^2+y^2}{2} + \frac{1-\mu}{r_{13}} + \frac{\mu}{r_{23}} \tag{4}$$

Because time does not explicitly appear in the equations of motion, the CR3BP supplies an autonomous dynamical model for approximating the natural motion of a spacecraft in a three-body system when formulated in the rotating frame. Furthermore, a wide variety of fundamental solutions exist including equilibrium points, periodic orbits, quasi-periodic orbits, and hyperbolic invariant manifolds.

3 Relative dynamics in a three-body system

The CR3BP is used in this section as a foundation for formulating the equations of relative motion between two spacecraft in a system with two massive primary bodies. Specifically, the target spacecraft, denoted by the subscript t, and the chaser spacecraft, denoted by the subscript c, are both assumed to follow uncontrolled natural reference paths in the CR3BP, assuming that the spacecraft do not gravitationally interact with each other. Nonlinear and linearized equations of relative motion are then presented for an observer in the rotating frame. The resulting equations of relative motion are autonomous, enabling an analysis of relative motion in the CR3BP independent of a specific epoch.

3.1 Nonlinear equations of relative motion in the CR3BP

An expression for the relative acceleration between two spacecraft, given an observer that is fixed in the rotating frame, is derived via a Newtonian approach. The position vector of the chaser spacecraft relative to the target spacecraft is denoted as $\boldsymbol{\rho}$, defined as $\boldsymbol{\rho} = \boldsymbol{r}_c - \boldsymbol{r}_t$, where $\boldsymbol{r}_t$ and $\boldsymbol{r}_c$ are the position vectors of the target and chaser spacecraft, respectively, measured from the P_1-P_2 barycenter. When expressed in the rotating frame, the components of this relative position vector are expressed as $\boldsymbol{\rho} = [\delta x, \delta y, \delta z]^T$. The inertial and nondimensional relative acceleration, $\ddot{\boldsymbol{\rho}}$, is then calculated as the difference between the inertial accelerations of the target and chaser spacecraft, each governed by Eq. (2), expressed as

$$\ddot{\boldsymbol{\rho}} = -\mu \left(\frac{\boldsymbol{r}_{2c}}{r_{2c}^3} - \frac{\boldsymbol{r}_{2t}}{r_{2t}^3} \right) - (1-\mu) \left(\frac{\boldsymbol{r}_{1c}}{r_{1c}^3} - \frac{\boldsymbol{r}_{1t}}{r_{1t}^3} \right) \tag{5}$$

The relative acceleration, $\boldsymbol{\rho}''$, between the two spacecraft for an observer fixed in the rotating frame is then calculated as

$$\boldsymbol{\rho}'' = \ddot{\boldsymbol{\rho}} - 2\Big(\boldsymbol{\omega}_{RN} \times \boldsymbol{\rho}'\Big) - \boldsymbol{\omega}_{RN} \times (\boldsymbol{\omega}_{RN} \times \boldsymbol{\rho}) \tag{6}$$

This second-order vector differential equation supplies the nonlinear equations of relative motion for the chaser spacecraft.

In the nonlinear system, the relative path of the chaser spacecraft is generated by simultaneously integrating the relative state of the chaser spacecraft and the absolute state of the target spacecraft; this approach straightforwardly supplies the information required to compute the presented local toroidal coordinate systems. A six-dimensional state vector, $\boldsymbol{q}$, is defined as the difference between the state vector of the chaser spacecraft, $\boldsymbol{x}_c$, and the state vector of the target spacecraft, $\boldsymbol{x}_t$, both formulated in the rotating frame, as $\boldsymbol{q} = \boldsymbol{x}_c - \boldsymbol{x}_t$. This relative state vector may be expressed as $\boldsymbol{q} = [\delta x, \delta y, \delta z, \delta \dot{x}, \delta \dot{y}, \delta \dot{z}]^T$. When the state of the target spacecraft is integrated via the equations of motion for the CR3BP in Eq. (1), and the relative state of the chaser spacecraft from the target spacecraft is simultaneously integrated via the equations of relative motion in Eq. (6), the paths of the two spacecraft are generated using a system of 12 scalar and autonomous first-order differential equations.

3.2 Linearized equations of relative motion

In this section, a first-order approximation of relative motion formulated in the rotating frame is presented for a target spacecraft located along a general reference trajectory in the CR3BP. However, in this paper, these expressions for the linearized equations of motion are applied to a target spacecraft that follows a periodic orbit in the CR3BP. These equations of relative motion that are linearized about a target spacecraft are written in the form

$$\boldsymbol{q}' \approx \boldsymbol{A}\big|_t \boldsymbol{q} = \left.\frac{\partial \boldsymbol{q}'}{\partial \boldsymbol{q}}\right|_t \boldsymbol{q} \tag{7}$$

where the Jacobian, $\boldsymbol{A}$, is evaluated at the state of the target spacecraft. This Jacobian is equal to the following matrix:

$$\boldsymbol{A}\big|_t = \begin{bmatrix} \boldsymbol{0}_3 & \boldsymbol{I}_3 \\ \left.\frac{\partial \rho''}{\partial \rho}\right|_t & \left.\frac{\partial \rho''}{\partial \rho'}\right|_t \end{bmatrix} \tag{8}$$

The lower-left quadrant of the Jacobian corresponds to the partial derivative of the relative acceleration for an observer in the rotating frame, expressed in Eq. (6), with respect to the relative position vector, written in nondimensional quantities as

$$\left.\frac{\partial \boldsymbol{\rho}''}{\partial \boldsymbol{\rho}}\right|_t = -\mu \left(\frac{\boldsymbol{I}_3}{r_{2t}^3} - \frac{3\boldsymbol{r}_{2t}\boldsymbol{r}_{2t}^T}{r_{2t}^5} \right) - (1-\mu) \left(\frac{\boldsymbol{I}_3}{r_{1t}^3} - \frac{3\boldsymbol{r}_{1t}\boldsymbol{r}_{1t}^T}{r_{1t}^5} \right) - \tilde{\boldsymbol{\omega}}_{RN}\tilde{\boldsymbol{\omega}}_{RN} \tag{9}$$

where $\tilde{\omega}_{RN}$ is the skew-symmetric matrix representation of the cross product of $\boldsymbol{\omega}_{RN}$ and $\boldsymbol{I}_n$ denotes the $n \times n$ identity matrix. Finally, the partial derivative of the relative acceleration for an observer in the rotating frame with respect to the relative velocity vector is equal to

$$\left.\frac{\partial \boldsymbol{\rho}''}{\partial \boldsymbol{\rho}'}\right|_t = -2\tilde{\omega}_{RN} \tag{10}$$

This vector partial derivative forms the lower-right quadrant of the Jacobian. Together, these quantities supply the components of the equations of relative motion that are linearized about a target spacecraft.

The first-order approximation of the relative path of a chaser spacecraft is generated by simultaneously integrating the relative state of the chaser spacecraft and absolute state of target spacecraft. A 12×1 system of equations is formed by the nonlinear equations of motion governing the target spacecraft state in the CR3BP, as expressed by Eq. (1), and the linearized equations of relative motion governing the relative state of the chaser spacecraft, as expressed in Eq. (7). The result is a system of 12 scalar and autonomous first-order differential equations where the motion of the target spacecraft is recovered to within the accuracy of numerical integration in the CR3BP and the motion of the chaser spacecraft is approximated via linearization about the target spacecraft.

4 Quasi-periodic relative motion

The coordinate systems introduced in this paper leverage a first-order approximation of an invariant 2-torus that exists in the linearized model of relative motion. This fundamental solution is used because a chaser spacecraft following the surface of a reference invariant 2-torus follows a quasi-periodic path relative to a target spacecraft on a nearby periodic orbit that admits an oscillatory mode. However, numerically calculating an invariant torus that exists in the nonlinear model is significantly more computationally intensive than calculating a periodic orbit. Thus, a first-order approximation of a torus, i.e., a torus that exists in the linearized model of relative motion, is used in this paper. As a result, the coordinate systems supply a straightforward and time-invariant state representation of motion on a first-order invariant torus and facilitate interpretation of motion in the nonlinear model. This approach of leveraging linearization has been used throughout the literature, including in support of analytical investigations for formation flying where the distance between spacecraft is sufficiently small (Carter 1998).

This section supplies an overview of the mathematical background for calculating a first-order approximation of quasi-periodic motion relative to a periodic orbit. First, a stability analysis of a periodic orbit is performed to supply basis vectors that span the center eigenspace associated with a single fixed point along a periodic orbit. These basis vectors are used to generate a first-order approximation of a nearby invariant 2-torus, i.e., a torus that is governed by two fundamental frequencies. The intersection of this torus with a hyperplane defines an invariant curve relative to a single fixed point. This section then presents a procedure for normalizing the basis vectors of the center eigenspace associated with a fixed point to align with the principal axes of a reference invariant curve. The resulting basis vectors supply the fundamental axes used to define the toroidal coordinate frames presented in this paper.

4.1 Stability analysis of a periodic orbit

A stability analysis is performed to recover basis vectors in the rotating frame for the eigenspaces associated with a periodic orbit in the CR3BP. Consistent with dynamical systems theory, stability analysis of a periodic orbit begins by numerically integrating the state transition matrix, $\boldsymbol{\Phi}$, from a specified fixed point, i.e., a state along a periodic orbit, that exists in the CR3BP (Breakwell and Brown 1979). The state transition matrix is governed by the matrix differential equation $d\boldsymbol{\Phi}/dt = \boldsymbol{A}\big|_t \boldsymbol{\Phi}$, using the initial conditions $\boldsymbol{\Phi}_0 = \boldsymbol{I}_6$, When this state transition matrix is propagated for precisely one period along a periodic orbit, it is denoted as the monodromy matrix. The eigenvalues of the monodromy matrix exist in three reciprocal or complex conjugate pairs, with one trivial pair of unity eigenvalues corresponding to periodicity of the reference solution (Howell 1984). The two nontrivial eigenvalue pairs then reflect the local stability characteristics of the periodic orbit (Koon et al. 2006): a pair of real eigenvalues that do not equal unity indicate stable and unstable modes, while a pair of complex conjugate eigenvalues on the unit circle indicates an oscillatory mode. The eigenvectors of the monodromy matrix then supply the span of the eigenspaces associated with a fixed point.

The stability of a periodic orbit is typically summarized using two stability indices. In this paper, a stability index is defined as the sum of a pair of two nontrivial eigenvalues of the monodromy matrix of the periodic orbit (Howell 1984). Because a trivial pair of eigenvalues of the monodromy matrix always exists, each orbit possesses two stability indices, denoted as s_1 and s_2. Oscillatory modes produce a value of the stability index between -2 and 2 (Gómez et al. 1998). Of course, a pair of complex eigenvalues that lie off the unit circle may also produce a value of the stability index between -2 and 2. However, this type of eigenvalue pair is not admitted by any of the periodic orbits examined in this investigation.

4.2 First-order approximation of an invariant 2-torus

A first-order approximation of an invariant 2-torus is calculated using the eigenvectors associated with an oscillatory mode of the monodromy matrix for a selected state along a periodic orbit. At this fixed point, a complex eigenvector associated with the oscillatory mode, $\boldsymbol{w}$, is used to generate a set of states $\boldsymbol{\varphi}$ that lie along a first-order approximation of an invariant 2-torus via the following expression:

$$\boldsymbol{\varphi} = \varepsilon \left(\mathrm{Re}(\boldsymbol{w}) \cos\theta + \mathrm{Im}(\boldsymbol{w}) \sin\theta\right) \tag{11}$$

where $\theta \in [0, 2\pi]$ radians and ε is a scaling term that influences the size of the first-order approximation of the nearby torus relative to the periodic orbit (Olikara and Scheeres 2012). For a constant value of ε, the real and imaginary vector components of the complex eigenvector associated with the oscillatory mode, labeled $\boldsymbol{w}_r$ and $\boldsymbol{w}_i$ such that $\boldsymbol{w} = \boldsymbol{w}_r + i\,\boldsymbol{w}_i$, are the directions of two conjugate diameters for the unique ellipse formed by the states within $\boldsymbol{\varphi}$ (McCartin 2013). This set of states $\boldsymbol{\varphi}$ is labeled a first-order approximation of an invariant curve: each state in this set returns to the same curve when propagated for one revolution around the torus (Barden and Howell 1999). o construct a first-order approximation of an invariant 2-torus relative to a periodic orbit, the complex eigenvector may be calculated at various states along one revolution of the periodic orbit by either integrating the eigenvector using the linear equations of relative motion or using mappings of the state transition matrix (Koon et al. 2006). Using this information, the set $\boldsymbol{\varphi}$ is computed at a constant value of ε at multiple locations along the periodic orbit. The resulting ellipses formed by the set $\boldsymbol{\varphi}$ for a constant value of ε may vary in size, eccentricity, and orientation over time, corresponding to an evolving geometry of the first-order approximation of the invariant torus relative to the periodic orbit (Barden and Howell 1999).

States in the set $\boldsymbol{\varphi}$ and, therefore, the center eigenspace associated with a specific fixed point lie within a two-dimensional plane in the six-dimensional phase space (Barden and Howell 1998b, 1999). The projection of the center eigenspace onto the configuration space forms a reference plane that is used to define the coordinate systems presented in this paper. Calculating this plane begins by writing the real and imaginary components of the complex eigenvector, $\boldsymbol{w}_r$ and $\boldsymbol{w}_i$, in terms of four 3×1 vectors corresponding to their position and velocity components as $\boldsymbol{w}_r = [\boldsymbol{r}_r^T, \boldsymbol{v}_r^T]^T$ and $\boldsymbol{w}_i = [\boldsymbol{r}_i^T, \boldsymbol{v}_i^T]^T$, respectively. The complex eigenvector may then be written as

$$\boldsymbol{w} = \begin{bmatrix} \boldsymbol{r}_r \\ \boldsymbol{v}_r \end{bmatrix} + \begin{bmatrix} \boldsymbol{r}_i \\ \boldsymbol{v}_i \end{bmatrix} i \tag{12}$$

For a single fixed point, $\boldsymbol{r}_r$ and $\boldsymbol{r}_i$ span the plane formed by the projection of the center eigenspace onto the configuration space. The unit vector perpendicular to this plane is defined as

$$\hat{\boldsymbol{n}} = \frac{\boldsymbol{n}}{n} = \frac{\boldsymbol{r}_r \times \boldsymbol{r}_i}{|\boldsymbol{r}_r \times \boldsymbol{r}_i|} \tag{13}$$

The orientation of the plane normal to $\hat{\boldsymbol{n}}$ is periodic in the rotating frame with the same period as the reference periodic orbit.

4.3 Normalization of the complex eigenvector

The real and imaginary vector components of the complex eigenvector of the monodromy matrix that is associated with the oscillatory mode supply a useful set of basis vectors for the center eigenspace. However, for consistent implementation when defining the local toroidal coordinate systems, a normalization scheme is applied to the complex eigenvector to remove ambiguity. The presented normalization process aligns the eigenvector with the principal axes of the first-order invariant curve approximation; constrains the magnitude of the real, position components of the eigenvector; and applies a series of sign checks to remove ambiguity in the sign of the real and imaginary components of the eigenvector at a specific fixed point along the periodic orbit.

The principal axes of the ellipse formed by the first-order approximation of the invariant curve are computed via a singular value decomposition (SVD) of a matrix containing columns that span the center eigenspace in the phase space. The mathematical concept of an SVD has been used in a variety of applications to gain geometric insight into flow properties, linear transformations, and data that exist within a hyperellipse; one example in astrodynamics is examining stretching distances between nearby trajectories using an SVD of the Cauchy-Green tensor (Short et al. 2015). In this paper, consider a fixed point of a periodic orbit that admits at least one oscillatory mode as indicated by the eigendecomposition of the monodromy matrix. One complex eigenvector from a complex conjugate pair that lies on the unit circle is selected, denoted as $\boldsymbol{w}^*$. Then, a $6{\times}2$ matrix is defined as $\boldsymbol{E} = [\mathrm{Re}(\boldsymbol{w}^*), \mathrm{Im}(\boldsymbol{w}^*)]$. The SVD of $\boldsymbol{E}$ is used to compute the lengths and directions of the principal axes of the ellipse formed by the invariant curve in terms of $\boldsymbol{w}^*$ (McCartin 2013). First, the matrix $\boldsymbol{E}$ is decomposed as $\boldsymbol{E} = \boldsymbol{U}\boldsymbol{\Sigma}\boldsymbol{V}^T$ (Noble and Daniel 1969). In this expression, the matrix $\boldsymbol{U}$ is a 6×2 semi-orthogonal matrix that contains basis vectors that are aligned with nonunique principal semi-axes of the ellipse formed by the invariant curve. Specifically, the columns of

$\boldsymbol{U}$ are ordered with the basis vector aligned with a semi-major axis of the ellipse formed by the invariant curve in the left column and the basis vector aligned with a semi-minor axis of the same ellipse in the right column. Note that in this context, the terminology semi-major axis is not related to the Keplerian orbital element; rather, the semi-major axis is associated with the ellipse formed by the invariant curve. The matrix $\boldsymbol{\Sigma}$ is a 2×2 diagonal matrix containing the magnitudes of the semi-major and semi-minor axes of the ellipse formed by the invariant curve in the upper-left and lower-right quadrants, respectively. Finally, the matrix $\boldsymbol{V}$ is a 2×2 orthogonal matrix, which may be expressed as a rotation matrix as (Noble and Daniel 1969)

$$\boldsymbol{V} = \begin{bmatrix} \cos\Theta & -\sin\Theta \\ \sin\Theta & \cos\Theta \end{bmatrix} \tag{14}$$

where Θ is the angle between the axes defined by the input eigenvector and the principal axes of the ellipse.

A complex scaling factor is applied to the complex eigenvector to recover basis vectors of the center eigenspace that are aligned with the principal axes of the ellipse formed by the invariant curve. Rearranging the SVD of $\boldsymbol{E}$ produces the relationship $\boldsymbol{E}\boldsymbol{V} = \boldsymbol{U}\boldsymbol{\Sigma}$. The right hand side of this expression, $\boldsymbol{U}\boldsymbol{\Sigma}$, is equivalent to a 6×2 matrix containing a vector $\boldsymbol{a}$ in the left column that is measured from the center of the ellipse formed by the invariant curve and directed along the major axis, as well as a vector $\boldsymbol{b}$ in the right column that is directed along the minor axis. This analysis reveals that the matrix $\boldsymbol{E}$, right multiplied by $\boldsymbol{V}$, is equal to the matrix $\boldsymbol{U}\boldsymbol{\Sigma}$ containing an orthogonal set of principal axes of the ellipse formed by the invariant curve. Accordingly, an eigenvector with real and imaginary components that are aligned with the principal axes of the ellipse formed by the invariant curve is computed by multiplying $\boldsymbol{w}^*$ by the complex scalar quantity $c = e^{-i\Theta}$, where Θ is extracted from $\boldsymbol{V}$. Scaling the complex eigenvector by c produces another complex eigenvector labeled $\boldsymbol{w}$ that forms a conjugate diameter description of the same ellipse described by $\boldsymbol{w}^*$. However, the real vector component of this eigenvector is aligned with the semi-major axis of the elliptical approximation of the invariant curve and the imaginary vector component is directed along the semi-minor axis, both measured from the fixed point at the center of the ellipse. This relationship between real and imaginary components of the complex eigenvector and the principal axes of the approximated invariant curve in the phase space is conceptually illustrated in the left subfigure of Fig. 1.

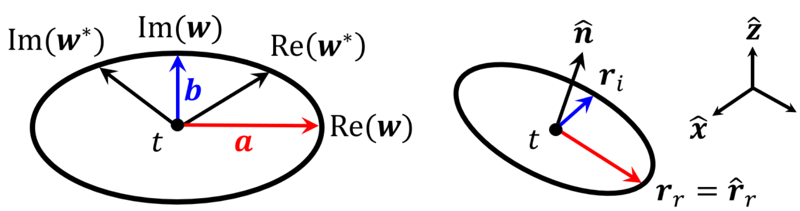

Fig. 1 Conceptual illustration of the normalization process applied to a complex eigenvector for consistent implementation of local toroidal coordinates: (left) alignment of real and imaginary components of the complex eigenvector with the principal axes of the approximated invariant curve and (right) orientation of the basis vectors in the three-dimensional configuration space

The real and imaginary components of the scaled complex eigenvector describe nonunique, principal semi-axes of an ellipse formed by an invariant curve of unspecified size relative to a fixed point. To capture the size of the ellipse formed by the first-order approximation of the invariant curve in configuration space, the complex eigenvector is scaled such that the magnitude of the projection of the semi-major axis of the ellipse onto the configuration space is equal to unity. Thus, the complex eigenvector is normalized such that the magnitude of $\boldsymbol{r}_r$ is equal to unity. As a result, the vector $\boldsymbol{r}_r$ forms a unit vector in configuration space and $\boldsymbol{r}_i$ possesses a magnitude of less than unity, consistent with the semi-minor axis of an ellipse possessing a smaller length than the semi-major axis. These two vectors, $\boldsymbol{r}_r$ and $\boldsymbol{r}_i$, are illustrated conceptually in the right subfigure of Fig. 1, along with the normal unit vector, $\hat{\boldsymbol{n}}$. This normalization step is useful within the definition of the local toroidal coordinate sets to aid interpretation of the size of an approximated invariant torus in the configuration space.

Finally, the sign ambiguities that occur within an SVD must be addressed via a series of sign checks to ensure a consistent definition for $\boldsymbol{w}$. However, because of the variety of geometries of periodic orbits that admit oscillatory modes, a single set of sign checks may not be effectively defined for general application across periodic orbits in the CR3BP. Rather, sign checks may be defined on a case-by-case basis. For example, for the analysis of the Earth-Moon southern L_2 halo orbit family included in Section 7, two sign checks are applied to the complex eigenvector calculated at apolune. First, if the perpendicular unit vector, $\hat{\boldsymbol{n}}$, computed via Eq. 13, is anti-parallel to the orbital angular momentum vector of the P_1-P_2 system (i.e., $\hat{\boldsymbol{n}}^T\hat{\boldsymbol{z}} < 0$), $\boldsymbol{w}$ is replaced with its complex conjugate. In addition, when evaluated at apolune along members of the Earth-Moon L_2 halo orbit family, $\boldsymbol{r}_r$ is observed to align with either $\hat{\boldsymbol{x}}$ or $\hat{\boldsymbol{y}}$ depending on the exact region of the orbit family. To define $\boldsymbol{r}_r$ along the positive direction of either axis, if $[1, 1, 0]^T\boldsymbol{r}_r < 0$, $-\boldsymbol{w}$ is used as the normalized eigenvector. The resulting components of the normalized complex eigenvector possess a unique and consistent description that is used within the mappings between relative Cartesian states and local toroidal coordinates. Note that the initial state along the periodic orbit where the complex eigenvector is computed and normalized must always be specified when using the toroidal coordinates systems presented in the following section to ensure consistent and repeatable implementation. Once normalized, this eigenvector is integrated via the Jacobian evaluated at states along the periodic orbit, or determined at a future fixed point via the state transition matrix.

5 Local toroidal coordinate systems

In this section, local toroidal coordinate systems are introduced to describe motion relative to a periodic orbit that admits an oscillatory mode in the CR3BP. These non-orthogonal coordinate systems are formulated using information about the center eigenspace to supply geometric insight into the relative state of a chaser spacecraft, while also possessing a consistent interpretation across various reference orbits. Specifically, for each coordinate system, three coordinates are used to decompose a relative position vector into its components within and normal to the plane of an instantaneously approximated invariant curve along a first-order approximation of a 2-torus. The time derivatives of these coordinates then supply further intuition into the deviation of the chaser spacecraft from motion tracing this reference 2-torus, which is described by constant values of the toroidal coordinates. The first coordinate set, denoted as the nonsingular local toroidal coordinates, possesses an oblique basis and maps linearly with Cartesian coordinates relative to a fixed point as a function of the complex eigenvector associated with an oscillatory mode. The second coordinate set, denoted as the geometric local toroidal coordinates, is a curvilinear system that expresses the state of the chaser spacecraft relative to a state along a periodic orbit using the amplitude and poloidal angle components of a reference 2-torus; this description is comparable to toroidal coordinates that are used to study magnetic fields and plasma physics (Hazeltine and Meiss 2003; Schnizer et al. 2014). However, in contrast to toroidal coordinate systems that describe a state measured from an origin on the revolution axis of the torus, the presented local toroidal coordinates are formulated to describe a state relative to a reference along the center ring of the torus, i.e., a state along the nearby periodic orbit in the CR3BP.

The toroidal coordinate sets presented in this paper to describe relative motion are defined using a single invariant 2-torus as a reference, i.e., a torus governed by two fundamental frequencies and generated by exciting one oscillatory mode. If a periodic orbit admits two oscillatory modes and, therefore, two sets of oscillatory modes of the monodromy matrix, higher-dimensional tori emanate from the periodic orbit. In this case, the approach presented in this paper requires that only one oscillatory mode is excited to construct the reference invariant 2-torus used to define the toroidal coordinate systems. This oscillatory mode may be selected based on its frequency or the size, shape, and evolution of the associated invariant curve. Further investigation and adaptation of the presented local toroidal coordinates to use a higher-order invariant torus as a reference represents an interesting avenue for future work. Furthermore, for some periodic orbits in the CR3BP, the orbit may admit an oscillatory mode that only spans a single dimension in the configuration space, e.g. the $\hat{z}$ axis. Motion exciting this type of mode is rectilinear in the configuration space and is not considered for analysis within the scope of this paper due to the resulting rank-deficiencies in the definition of the introduced coordinate systems. Finally, the local toroidal coordinates are presented via mappings from relative states formulated in the rotating frame; however, it is also valid to map to the introduced coordinates from other frames where the periodic orbit maintains periodicity, such as a Hill frame.

5.1 Nonsingular local toroidal coordinates

The nonsingular local toroidal coordinates are defined as three scalar quantities that, along with their respective time derivatives, describe the state of the chaser spacecraft relative to a target spacecraft located along a periodic orbit using basis vectors derived from the center eigenspace. The first and second coordinates, defined as α and β, express part of the relative position as a linear combination of the real and imaginary position components, $\boldsymbol{r}_r$ and $\boldsymbol{r}_i$, respectively, of the normalized complex eigenvector associated with the oscillatory mode evaluated at the state of the target spacecraft along the periodic orbit. The third coordinate, h, is defined as the distance of the chaser spacecraft from the plane spanning the projection of the center eigenspace onto the configuration space; a value of $h = 0$ indicates the chaser spacecraft is located within this plane. For a nonzero value of h, the sign reflects whether the relative position vector of the chaser spacecraft is parallel or anti-parallel to $\hat{\boldsymbol{n}}$, the unit vector that is normal to the plane formed by the projection of the center eigenspace onto the configuration space. Each coordinate is specified with dimensions of length and may be nondimensionalized using the characteristic length quantity associated with the CR3BP. Figure 3 displays a conceptual illustration of nonsingular local toroidal coordinates, (α, β, h), associated with the relative position vector, $\boldsymbol{\rho}$, measured from a target spacecraft, t, located on a periodic orbit to a chaser spacecraft, c, along with the basis vectors, $\{\boldsymbol{r}_r, \boldsymbol{r}_i, \hat{\boldsymbol{n}}\}$.

The nonsingular toroidal coordinate frame is a nonorthogonal reference frame that possesses basis vectors that do not necessarily possess unit length. The basis vectors are defined as the real and imaginary position components of the normalized complex eigenvector associated with the oscillatory mode of a nearby state along a periodic orbit as well as the unit

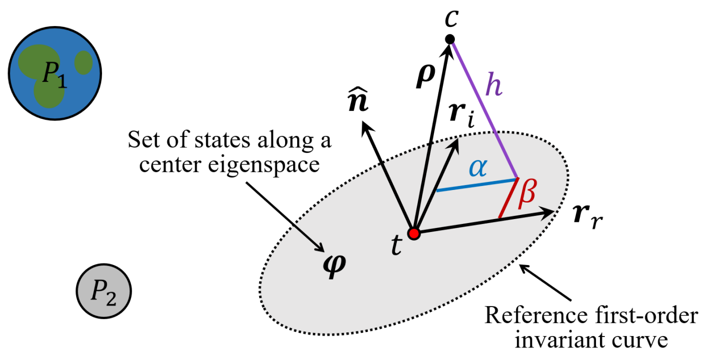

Fig. 2 Illustration of the nonsingular local toroidal coordinates (α,β,h) describing the position of the chaser spacecraft relative to a target spacecraft located on a periodic orbit with an oscillatory mode

vector that is normal to the corresponding plane. These vectors, $\{\boldsymbol{r}_r, \boldsymbol{r}_i, \hat{\boldsymbol{n}}\}$, form the axes of the nonsingular toroidal coordinate frame, denoted $\mathcal{Z}$. Because of their definition, these basis vectors must be carefully and consistently computed over the time interval of interest. Specifically, recall that as a result of the normalization process detailed in Section 4.3, the magnitude of $\boldsymbol{r}_r$ is equal to unity at a specified initial epoch when calculated using a single initial state along the periodic orbit. However, the magnitudes of the basis vectors $\boldsymbol{r}_r$ and $\boldsymbol{r}_i$ are designed to vary at later instants of time, consistent with the invariant curve associated with a single invariant torus also evolving in size and shape relative to subsequent states along the reference periodic orbit. Thus, the normalized complex eigenvector used to compute the basis vectors within this system is integrated along with the state of the target spacecraft from a specified initial condition via the Jacobian matrix to capture the natural rotational frequencies of the center eigenspace.

The position vector locating the chaser spacecraft relative to a state along a periodic orbit may be expressed using nonsingular coordinates. The relative position vector, $\boldsymbol{\rho}$, is written in terms of the nonsingular toroidal coordinates as

$$\boldsymbol{\rho} = \alpha \boldsymbol{r}_r + \beta \boldsymbol{r}_i + h\hat{\boldsymbol{n}} \tag{15}$$

The position of the chaser spacecraft relative to a fixed point may also be expressed in nonsingular toroidal coordinates via the vector $\boldsymbol{z} = [\alpha, \beta, h]^T$. The time derivative of the nonsingular coordinates for an observer fixed in the toroidal coordinate frame, indicated by the notation ${}^{\mathcal{Z}}(\ )'$, is defined as ${}^{\mathcal{Z}}\boldsymbol{z}' = [\dot{\alpha}, \dot{\beta}, \dot{h}]^T$ whereas the second time derivative is defined as ${}^{\mathcal{Z}}\boldsymbol{z}'' = [\ddot{\alpha}, \ddot{\beta}, \ddot{h}]^T$.

To calculate the nonsingular toroidal coordinates, a transformation is employed between the non-orthogonal toroidal coordinate frame and Cartesian coordinates in the rotating frame. The vector, $\boldsymbol{z}$, is defined as the relative position vector describing the chaser spacecraft measured from the periodic orbit expressed in the nonsingular local toroidal coordinate frame. Thus, the nonsingular local toroidal coordinates are computed via a change of basis, written as

$$\boldsymbol{\rho} = \boldsymbol{R}\boldsymbol{z} \tag{16}$$

where $\boldsymbol{R}$ is a 3×3 matrix containing the basis vectors of the nonsingular toroidal coordinate system expressed in the rotating frame, defined as $\boldsymbol{R} = [\boldsymbol{r}_r, \boldsymbol{r}_i, \hat{\boldsymbol{n}}]$ where $\boldsymbol{r}_r$ and $\boldsymbol{r}_i$ are the real and imaginary position components of the normalized complex eigenvector which has been integrated from the specified initial fixed point and evaluated at the current state of the target spacecraft along the periodic orbit. The nonsingular coordinates are then straightforwardly determined by inverting $\boldsymbol{R}$ as

$$z = \boldsymbol{R}^{-1}\boldsymbol{\rho} \tag{17}$$

The matrix $\boldsymbol{R}$ is full rank and invertible so long as $\boldsymbol{r}_r$ and $\boldsymbol{r}_i$ are not collinear; this condition is satisfied when the oscillatory mode of a periodic orbit does not produce rectilinear motion in its associated Cartesian frame. Computing the time derivative of Eq. (16), the relative velocity of the chaser spacecraft, $\boldsymbol{\rho}'$, is written as a function of the coordinates and coordinate rates as

$$\boldsymbol{\rho}' = \boldsymbol{R}\left({}^{\mathcal{Z}}z'\right) + \boldsymbol{R}'z \tag{18}$$

where $\boldsymbol{R}'$ is the time derivative of the $\boldsymbol{R}$ matrix for an observer in the rotating frame, written as $\boldsymbol{R}' = [\boldsymbol{v}_r, \boldsymbol{v}_i, \hat{\boldsymbol{n}}']$ where each component is derived from the normalized complex eigenvector which has been integrated from the specified initial fixed point and evaluated at the current state of the target spacecraft along the periodic orbit. In this expression, the time derivative of the normal unit vector for an observer in the rotating frame, $\hat{\boldsymbol{n}}'$, is calculated as

$$\hat{\boldsymbol{n}}' = \frac{\boldsymbol{n}'}{n} - \left(\boldsymbol{n}^T\boldsymbol{n}'\right)\frac{\boldsymbol{n}}{n^3} \tag{19}$$

where $\boldsymbol{n}' = \boldsymbol{v}_r \times \boldsymbol{r}_i + \boldsymbol{r}_r \times \boldsymbol{v}_i$. The time derivative of the nonsingular coordinate set for an observer in the $\mathcal{Z}$ frame is then computed as a function of relative Cartesian position and velocity vectors as

$${}^{\mathcal{Z}}z' = \boldsymbol{R}^{-1}\boldsymbol{\rho}' - \boldsymbol{R}^{-1}\boldsymbol{R}'\boldsymbol{R}^{-1}\boldsymbol{\rho} \tag{20}$$

This expression describes a transformation between the velocity vector for an observer fixed in the rotating frame to the velocity vector for an observer fixed in the non-orthogonal toroidal coordinate system.

5.2 Geometric local toroidal coordinates

The geometric local toroidal coordinates modify the nonsingular local toroidal coordinates to express the state of the chaser spacecraft in terms of geometrically-interpretable quantities. The first coordinate, ε, indicates the size of the first-order approximation of the invariant curve that passes through the projection of the relative position vector of the chaser spacecraft onto the plane instantaneously spanned by $\boldsymbol{r}_r$ and $\boldsymbol{r}_i$. The ε coordinate is always positive and is expressed using length units. The second coordinate, θ, indicates the angular displacement of the chaser spacecraft about the ellipse formed by the first-order approximation of the invariant curve in configuration space, measured within the plane spanned by $\boldsymbol{r}_r$ and $\boldsymbol{r}_i$. Specifically, the angle is measured counterclockwise from $\boldsymbol{r}_r$ when viewed from the $\hat{\boldsymbol{n}}$ direction. The ε and θ coordinates are related to the nonsingular coordinates, α and β, as

$$\alpha = \varepsilon\cos\theta \tag{21}$$

$$\beta = \varepsilon\sin\theta \tag{22}$$

The last coordinate, h, possesses the same definition as in the nonsingular coordinate system. Note that when the eigenvector normalization scheme described in Section 4 is applied, ε is equal to the maximum separation distance of the first-order approximation of the invariant curve from a specified initial fixed point along a periodic orbit. In some cases, it may be useful to specify this initial condition as a geometrically-meaningful fixed point. For example, if the normalized eigenvector is defined at an apsis of a periodic orbit, the physical interpretation of ε is the maximum separation distance of the approximated invariant curve defined by ε relative to the apsis. A conceptual illustration of these geometric toroidal coordinates (ε, θ, h) that describe the configuration of a chaser spacecraft relative to a target spacecraft located along a periodic orbit is displayed in Fig. 3.

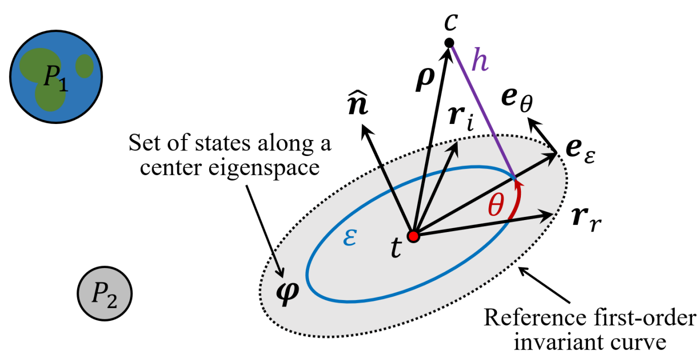

Fig. 3 Illustration of the geometric local toroidal coordinates (ε,θ,h) describing the position of the chaser spacecraft relative to a target spacecraft located on a periodic orbit with an oscillatory mode

The geometric toroidal coordinate system is a local, curvilinear coordinate system with basis vectors that are aligned with the amplitude, angle, and axial components of a reference invariant 2-torus. The geometric toroidal coordinate frame, $\mathcal{E}$, is defined with axes $\{\boldsymbol{e}_\varepsilon, \boldsymbol{e}_\theta, \hat{\boldsymbol{n}}\}$, calculated as a function of both the complex eigenvector associated with the oscillatory mode and geometric coordinates as

$$\boldsymbol{e}_\varepsilon = \boldsymbol{r}_r \cos\theta + \boldsymbol{r}_i \sin\theta, \qquad \boldsymbol{e}_\theta = \varepsilon\left(-\boldsymbol{r}_r \sin\theta + \boldsymbol{r}_i \cos\theta\right) \tag{23}$$

Representations of these axes are also illustrated in Fig. 3. Consistent with the nonsingular coordinate frame, the basis vectors are nonorthogonal, and the magnitudes of $\boldsymbol{e}_\varepsilon$ and $\boldsymbol{e}_\theta$ are generally not equal to unity. Unlike the nonsingular coordinates, the geometric coordinates do not map to relative position vectors as a linear combination of the basis vectors. However, it is convenient to express the values of the geometric toroidal coordinates in a 3×1 column vector, $\boldsymbol{e} = [\varepsilon, \theta, h]^T$. The first and second time derivatives of the geometric toroidal coordinates are similarly grouped in 3×1 column vectors as ${}^{\mathcal{E}}\boldsymbol{e}' = [\dot{\varepsilon}, \dot{\theta}, \dot{h}]^T$ and ${}^{\mathcal{E}}\boldsymbol{e}'' = [\ddot{\varepsilon}, \ddot{\theta}, \ddot{h}]^T$, respectively. Compared to the nonsingular coordinate set, the geometric toroidal coordinates supply increased intuition into the position of the chaser spacecraft, at the expense of a singular point along the $\hat{\boldsymbol{n}}$ axis. Along the $\hat{\boldsymbol{n}}$ axis, $\varepsilon = 0$ and a nonunique definition occurs in the mapping from geometric toroidal coordinates to Cartesian coordinates. When this condition is met, θ is undefined.

The values of the geometric toroidal coordinates are directly computed from the nonsingular coordinates. Once the nonsingular coordinates have been computed from the position and velocity vectors of a chaser spacecraft relative to a target spacecraft located along a periodic orbit via Eqs. (17) and (20), ε and θ are extracted as

$$\varepsilon = \sqrt{\alpha^2 + \beta^2}, \tag{24}$$

$$\theta = \tan^{-1}\left(\frac{\beta}{\alpha}\right) \tag{25}$$

The geometric coordinate rates are calculated as nonlinear functions of the nonsingular coordinates and their respective rates as

$$\dot{\varepsilon} = \frac{\alpha\dot{\alpha} + \beta\dot{\beta}}{\varepsilon}, \tag{26}$$

$$\dot{\theta} = \frac{\alpha\dot{\beta} - \beta\dot{\alpha}}{\varepsilon^2} \tag{27}$$

The values of the coordinate h and its time derivative $\dot{h}$ remain unchanged from the nonsingular coordinate set. The position vector is written as a nonlinear function of the geometric toroidal coordinates as

$$\boldsymbol{\rho} = \varepsilon\left(\boldsymbol{r}_r \cos\theta + \boldsymbol{r}_i \sin\theta\right) + h\hat{\boldsymbol{n}} \tag{28}$$

The time derivative of Eq. (28) produces an expression for the relative velocity of the chaser spacecraft, $\boldsymbol{\rho}'$, in terms of the the geometric coordinates and their rates as

$$\boldsymbol{\rho}' = \dot{\varepsilon}\big(\boldsymbol{r}_r \cos\theta + \boldsymbol{r}_i \sin\theta\big) + \varepsilon\big(\boldsymbol{v}_r \cos\theta - \boldsymbol{r}_r \sin\theta\dot{\theta} + \boldsymbol{v}_i \sin\theta + \boldsymbol{r}_i \cos\theta\dot{\theta}\big) + \dot{h}\hat{\boldsymbol{n}} + h\hat{\boldsymbol{n}}' \tag{29}$$

These expressions map the geometric local toroidal coordinates and respective coordinate rates to the relative position and velocity vectors expressed in the rotating frame and relative to a state along a periodic orbit.

5.3 Properties of quasi-periodic motion in local toroidal coordinates

While a relative state may be expressed via the local toroidal coordinate systems, states within the set $\boldsymbol{\varphi}$ that lie along the first-order approximation of an invariant curve are straightforward to describe via a sparse state representation where only two of the six coordinates and coordinate rates possess nonzero values. This section demonstrates that states within the set $\boldsymbol{\varphi}$ are equilibrium solutions to the equations of relative motion that are linearized relative to a periodic orbit when expressed using local toroidal coordinates. This result is a direct consequence of defining the basis vectors of the local toroidal coordinate frames using the normalized complex eigenvector associated with the oscillatory mode, which is integrated along with the state of the target spacecraft. In nonsingular toroidal coordinates, all states within the set $\boldsymbol{\varphi}$ admit values of $h = \dot{h} = \dot{\alpha} = \dot{\beta} = 0$, while α and β are free parameters indicating the projection of the position vector onto the plane instantaneously spanned by $\boldsymbol{r}_r$ and $\boldsymbol{r}_i$. This property of the coordinate set is evident in Eqs. (15) and (18), where $h = \dot{h} = \dot{\alpha} = \dot{\beta} = 0$ results in a state along the set $\boldsymbol{\varphi}$ as defined in Eq. (11). Similarly, in geometric toroidal coordinates, all states within the set $\boldsymbol{\varphi}$ possess values of $h = \dot{h} = \dot{\varepsilon} = \dot{\theta} = 0$ due to the definitions of the geometric coordinates as a function of the nonsingular coordinates, expressed in Eqs. (24)-(27). The quantities ε and θ are analogous free parameters that, respectively, correspond to the size of and angle along the first-order approximation of the invariant curve associated with a fixed point.

The equations of relative motion that are linearized about a periodic orbit and the time derivative of the normalized complex eigenvector, $\boldsymbol{w}$, are both governed by the Jacobian evaluated along the periodic orbit. The Jacobian evaluated at a state along a periodic orbit may be expressed using four 3×3 submatrices as

$$\boldsymbol{A}\big|_t = \begin{bmatrix} \boldsymbol{A}_1 & \boldsymbol{A}_2 \\ \boldsymbol{A}_3 & \boldsymbol{A}_4 \end{bmatrix} \tag{30}$$

The time derivative of the eigenvector $\boldsymbol{w}$ for an observer in the rotating frame is then written as the sum of two 6×1 vectors containing the real and imaginary components as $\boldsymbol{w}' = \boldsymbol{w}_r' + i\,\boldsymbol{w}_i'$. These two vectors are each defined in terms of two, three-dimensional vectors corresponding to relative velocity and acceleration as $\boldsymbol{w}_r' = [\boldsymbol{v}_r^T, \boldsymbol{a}_r^T]^T$ and $\boldsymbol{w}_i' = [\boldsymbol{v}_i^T, \boldsymbol{a}_i^T]^T$, where $\boldsymbol{v}$ and $\boldsymbol{a}$ indicate velocity and acceleration components of the eigenvector, respectively, and the subscripts r and i indicate real and imaginary components, respectively. Using these definitions, $\boldsymbol{a}_r$ and $\boldsymbol{a}_i$, are then expressed as linear functions of the submatrices of the Jacobian as $\boldsymbol{a}_r = \boldsymbol{A}_3\boldsymbol{r}_r + \boldsymbol{A}_4\boldsymbol{v}_r$ and $\boldsymbol{a}_i = \boldsymbol{A}_3\boldsymbol{r}_i + \boldsymbol{A}_4\boldsymbol{v}_i$, respectively.

An expression for the relative acceleration of a state within the set $\boldsymbol{\varphi}$ is derived by expressing the equations of relative motion that are linearized about a periodic orbit in terms of toroidal coordinates and the Jacobian. The linearized relative Cartesian acceleration is approximated as a function of the submatrices of the Jacobian and the relative position and velocity vectors as

$$\boldsymbol{\rho}'' \approx \boldsymbol{A}_3\boldsymbol{\rho} + \boldsymbol{A}_4\boldsymbol{\rho}' \tag{31}$$

Recall that the relative position vector for a state within the set $\boldsymbol{\varphi}$ in terms of nonsingular coordinates is written as $\boldsymbol{\rho}|_{\varphi} = \alpha\boldsymbol{r}_r + \beta\boldsymbol{r}_i$ whereas the associated relative velocity vector for an observer fixed in the rotating frame is written as $\boldsymbol{\rho}'|_{\varphi} = \alpha\boldsymbol{v}_r + \beta\boldsymbol{v}_i$. Substituting the expressions for these relative position and velocity vectors into the expression for the linearized relative acceleration of the chaser spacecraft in Eq. (31), the relative acceleration of a state along the first-order approximation of the invariant curve is written as

$$\boldsymbol{\rho}''\big|_{\varphi} \approx \boldsymbol{A}_3\left(\alpha\boldsymbol{r}_r + \beta\boldsymbol{r}_i\right) + \boldsymbol{A}_4\left(\alpha\boldsymbol{v}_r + \beta\boldsymbol{v}_i\right) = \alpha\boldsymbol{a}_r + \beta\boldsymbol{a}_i \tag{32}$$

Accordingly, this expression relates the acceleration for a state located along the first-order approximation of the invariant curve to the time derivative of the complex eigenvector and the nonsingular coordinates, α and β.

An expression for the second time derivative of the nonsingular toroidal coordinates evaluated on the set $\boldsymbol{\varphi}$ is derived and used to prove that the set corresponds to an equilibrium solution to the equations of relative motion linearized about a periodic orbit. First, recall the expression for the relative velocity, $\boldsymbol{\rho}'$, in terms of nonsingular coordinates and coordinate rates in Eq. (18). Differentiating Eq. (18) with respect to time produces an expression for the relative acceleration for an observer fixed in the rotating frame, $\boldsymbol{\rho}''$, in terms of nonsingular coordinates and coordinate rates as

$$\boldsymbol{\rho}'' = \boldsymbol{R}''z + 2\boldsymbol{R}'\left({}^{\mathcal{Z}}z'\right) + \boldsymbol{R}\left({}^{\mathcal{Z}}z''\right) \tag{33}$$

where $\boldsymbol{R}''$ is the second time derivative of $\boldsymbol{R}$, equal to $\boldsymbol{R}'' = [\boldsymbol{a}_r, \boldsymbol{a}_i, \hat{\boldsymbol{n}}'']$. Solving for ${}^{\mathcal{Z}}\boldsymbol{z}''$, the second time derivative of the nonsingular coordinates is then equal to

$$^{\mathcal{Z}}z'' = \boldsymbol{R}^{-1}\left(\boldsymbol{\rho}'' - \boldsymbol{R}''z - 2\boldsymbol{R}'\left({}^{\mathcal{Z}}z'\right)\right) \tag{34}$$

Recall that for states within the set $\boldsymbol{\varphi}$, the coordinate rates for an observer fixed in the $\mathcal{Z}$ frame, i.e., ${}^{\mathcal{Z}}\boldsymbol{z}'$, and the out-of-plane coordinate, h, are equal to zero. Consequently, the second time derivative of the geometric coordinate set evaluated along $\boldsymbol{\varphi}$ simplifies to

$$^{\mathcal{Z}}z''\big|_{\varphi} = \boldsymbol{R}^{-1}\left(\boldsymbol{\rho}''\big|_{\varphi} - \alpha\boldsymbol{a}_r - \beta\boldsymbol{a}_i\right) \tag{35}$$

Substituting Eq. (32), the expression for the linearized relative acceleration of the chaser spacecraft evaluated at a state within the set $\boldsymbol{\varphi}$, reveals that

$$^{\mathcal{Z}}z''\big|_{\varphi} \approx \boldsymbol{R}^{-1}\left(\alpha\boldsymbol{a}_r + \beta\boldsymbol{a}_i - \alpha\boldsymbol{a}_r - \beta\boldsymbol{a}_i\right) = \boldsymbol{0} \tag{36}$$

Because the first and second time derivatives of the geometric coordinates equal zero, a state within the set $\boldsymbol{\varphi}$ corresponds to an equilibrium solution to the equations of relative motion linearized about a periodic orbit. This result supplies a direct description of trajectories in the linear equations of relative motion that trace out the surface of a first-order approximation of an invariant torus via toroidal coordinates.

6 Computing separation extrema for relative motion along a torus

At a constant value of ε, states in the set $\boldsymbol{\varphi}$ form an ellipse in the three-dimensional configuration space relative to the associated fixed point along a periodic orbit. For this fixed point, the principal semi-axes of this ellipse in configuration space correspond to the instantaneous extrema in the position separation between a target spacecraft following a periodic orbit and a chaser spacecraft located on the first-order approximation of the invariant curve for a specific value of ε. This result offers valuable information in the preliminary design of spacecraft formations using quasi-periodic motion and subject to constraints on inter-spacecraft separation.

The states located at the vertices and co-vertices of the first-order approximation of the invariant torus are directly computed by integrating the components of an SVD. First, the normalized complex eigenvector formulated in the rotating frame is calculated at a specified fixed point along a periodic orbit. Next, a 3×2 matrix, $\boldsymbol{E}_r$, is defined using the real and imaginary position components of the complex eigenvector as $\boldsymbol{E}_r = \varepsilon[\boldsymbol{r}_r, \boldsymbol{r}_i]$, where ε reflects the size of the approximated invariant torus. This matrix is decomposed via an SVD as $\boldsymbol{E}_r = \boldsymbol{U}_r \boldsymbol{\Sigma}_r \boldsymbol{V}_r^T$, where $\boldsymbol{U}_r$ is a 3×2 semi-orthogonal matrix containing the basis unit vectors of the principal axes in configuration space. Specifically, $\boldsymbol{U}_r$ is ordered with a unit vector aligned with a major axis in the left column and a unit vector aligned with a minor axis in the right columns. The matrix $\boldsymbol{\Sigma}_r$ is a 2×2 diagonal matrix containing the magnitude of the semi-major axis, r_a, and the magnitude of the semi-minor axis, r_b, of the ellipse in the upper-left and lower-right, respectively. The matrix elements of the SVD of the matrix, $\boldsymbol{E}_r$, then are differentiated as (Seeger et al. 2017; Townsend 2016)

$$\frac{d}{dt}\boldsymbol{U}_r = \boldsymbol{U}_r \left(\boldsymbol{F} \circ \left(\boldsymbol{U}_r^T \boldsymbol{E}_r' \boldsymbol{V}_r \boldsymbol{\Sigma}_r + \boldsymbol{\Sigma}_r \boldsymbol{V}_r^T (\boldsymbol{E}_r')^T \boldsymbol{U}_r\right)\right) + \left(\boldsymbol{I}_3 - \boldsymbol{U}_r \boldsymbol{U}_r^T\right) \boldsymbol{E}_r' \boldsymbol{V}_r \boldsymbol{\Sigma}_r^{-1} \tag{37a}$$

$$\frac{d}{dt}\boldsymbol{\Sigma}_r = \boldsymbol{I}_2 \circ \left(\boldsymbol{U}_r^T \boldsymbol{E}_r' \boldsymbol{V}_r\right) \tag{37b}$$

$$\frac{d}{dt}\boldsymbol{V}_r = \boldsymbol{V}_r \left(\boldsymbol{F} \circ \left(\boldsymbol{\Sigma}_r \boldsymbol{U}_r^T \boldsymbol{E}_r' \boldsymbol{V}_r + \boldsymbol{V}_r^T (\boldsymbol{E}_r')^T \boldsymbol{U}_r \boldsymbol{\Sigma}_r\right)\right) + \left(\boldsymbol{I}_2 - \boldsymbol{V}_r \boldsymbol{V}_r^T\right) (\boldsymbol{E}_r')^T \boldsymbol{U}_r \boldsymbol{\Sigma}_r^{-1} \tag{37c}$$

where $\boldsymbol{F}$ is a 2×2 matrix function of the instantaneous values of r_a and r_b, defined as (Townsend 2016)

$$\boldsymbol{F} = \begin{bmatrix} 0 & \frac{1}{r_b^2 - r_a^2} \\ \frac{1}{r_a^2 - r_b^2} & 0 \end{bmatrix} \tag{38}$$

To support the integration of the SVD of $\boldsymbol{E}_r$, its time derivative is defined as $\boldsymbol{E}_r' = \varepsilon[\boldsymbol{v}_r, \boldsymbol{v}_i]$. The matrix components of the SVD of $\boldsymbol{E}_r$, i.e. $\boldsymbol{U}_r$, $\boldsymbol{\Sigma}_r$, and $\boldsymbol{V}_r$, are simultaneously integrated via the matrix differential equations in Eq. (37) together with the state of the target spacecraft and the complex eigenvector associated with the oscillatory mode. The vectors that appear in the columns of $(\boldsymbol{U}_r \boldsymbol{\Sigma}_r)$ locate a vertex and co-vertex of the first-order approximation of an invariant curve. The other vertex and co-vertex of the invariant curve are straightforwardly calculated by mirroring the computed principal axes across the origin, i.e., a fixed point along the periodic orbit.

The sequence of relative position vectors directed towards the vertices and co-vertices of the ellipse as it evolves over time does not correspond to a natural trajectory. Rather, the principal axes are geometric characteristics of the approximated invariant curve, governed by the differential equations in Eq. (37); they do not correspond to a continuous sequence of states generated using the linearized relative dynamics expressed in Eq. (7). Accordingly, a spacecraft initially aligned with the semi-major axis of the elliptical approximation of an invariant curve will not necessarily be located along the semi-major axis of the ellipse relative to a subsequent fixed point at a later instant of time.

Integrating the SVD of the first-order approximation of the invariant curve for a revolution of the periodic orbit reveals fundamental insight into the separation between the target and chaser spacecraft. While this process supplies the separation distance extrema over time for the first-order approximation of an invariant torus, for small spacecraft separations, nonlinear motion initialized on the invariant curve is demonstrated in the next section to be well-approximated by these extrema. This process may also be modified to compute the first-order approximation of the relative velocity magnitude between the chaser spacecraft exhibiting quasi-periodic relative motion and the target spacecraft located along a periodic orbit. In this case, the initial SVD is performed on the matrix containing columns composed of the real and imaginary velocity components of the complex eigenvector.

7 Quasi-periodic relative motion near the Earth-Moon L_2 southern halo orbit family

In this section, the presented toroidal coordinates and associated techniques are used to analyze first-order approximations of quasi-periodic relative motion near members of the L_2 southern halo orbit family in the Earth-Moon CR3BP. This section begins with a stability analysis of the Earth-Moon L_2 southern halo orbit family to identify members that admit oscillatory modes and, therefore, nearby quasi-periodic relative motion. A single member of this family is also identified to facilitate a detailed demonstration of the technical procedures presented in this paper prior to expansion to other members of the family. Next, first-order approximations of invariant 2-tori are generated using toroidal coordinates near various members of this family and visualized in the rotating frame. An error analysis is then performed to compare the trajectories generated in the nonlinear and linear models from the same initial conditions associated with first-order approximations of quasi-periodic relative motion. This error analysis is performed for various members of the L_2 southern halo orbit family for tori of various sizes and represented using the geometric toroidal coordinate set to facilitate interpretation. Finally, first-order approximations of invariant tori near various members of the L_2 southern halo orbit family are characterized by their minimum and maximum separation from the nearby periodic orbit using the principal axes of invariant curves calculated relative to various fixed points. This final example demonstrates the capacity for the toroidal coordinates to facilitate rapid examination of the separations between spacecraft within a formation that are following naturally bounded motion.

7.1 First-order approximations of invariant tori near the L_2 southern halo orbit family

In the Earth-Moon CR3BP, members of the L_2 southern halo orbit family evolve away from a bifurcation with the L_2 Lyapunov orbit family and towards the Moon, possessing a maximum

z-extension that occurs below the Earth-Moon plane (Breakwell and Brown 1979; Farquhar 1971). In Fig. 4, selected members of the southern L_2 halo orbit family are plotted in the Earth-Moon rotating frame using dimensional coordinates measured relative to the Moon. Four specific halo orbits within this family are highlighted in Fig. 4 and used later in this subsection to demonstrate the characteristics of nearby invariant 2-tori.

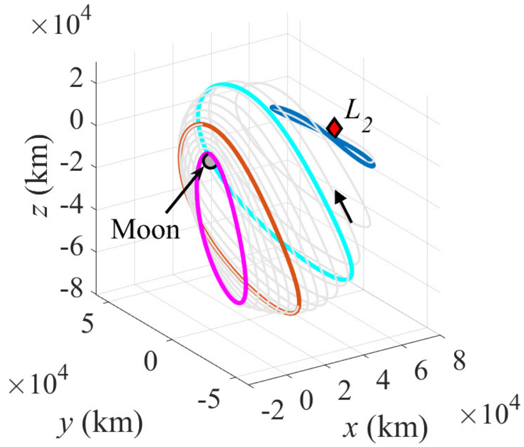

Fig. 4 Members of the Earth-Moon southern L_2 halo orbit family plotted relative to the Moon in the Earth-Moon rotating frame

To facilitate a detailed initial demonstration of the technical approach presented in this paper, an Earth-Moon L_2 southern halo orbit with a period of 13.3 days is examined. This particular periodic orbit is displayed in cyan in Fig. 4 and possesses a nondimensional state at apolune in the rotating frame of approximately $\boldsymbol{x} = [1.1358, 0, -0.16938, 0, -0.22465, 0]^T$. From this state at apolune, a monodromy matrix is generated by propagating the state transition matrix in the rotating frame for one period, i.e., approximately 13.3 days. This monodromy matrix admits the following eigenvalue structure: a trivial unity eigenvalue pair, $\lambda_{1,2}$; a pair of unstable and stable modes, $\lambda_{3,4}$; and a pair of complex conjugate eigenvalues that lies on the unit circle, $\lambda_{5,6}$, corresponding to an oscillatory mode. The nontrivial eigenvalues of the monodromy matrix and the associated eigenvectors are listed in Table 1. For the presented analysis, the oscillatory mode is of particular interest. Specifically, the complex eigenvector following the normalization process is listed in Table 1 as $\boldsymbol{w}_6$. This normalized complex eigenvector is used to recover a nearby first-order invariant 2-torus used as a reference in the computation of the local toroidal coordinates.

A first-order approximation of an invariant 2-torus is generated near the 13.3 day southern L_2 halo orbit for demonstration. First, a discrete number of states that lie along a single invariant curve are calculated via Eq. (11) relative to apolune along the reference halo orbit. For this example, 200 evenly distributed values of θ at $\varepsilon = 1$ km are used. The left subfigure of Fig. 5 displays a projection of the resulting invariant curve onto the configuration space of the rotating frame. This approximated invariant curve is plotted relative to apolune along the L_2 halo orbit, indicated as a red marker at the origin and labeled as t. The real and imaginary position components of the normalized complex eigenvector associated with the oscillatory mode are also plotted as red and blue arrows, respectively. This information is

Table 1 Nontrivial eigenvalues and eigenvectors of the monodromy matrix evaluated at apolune of the selected Earth-Moon L_2 halo orbit and expressed in the rotating frame

$\lambda_3 = 102.28$	$\lambda_4 = 9.78 \times 10^{-3}$	$\lambda_{5,6} = -0.514 \pm 0.858i$
$\boldsymbol{w}_3 = \begin{bmatrix} -0.4579 \\ 0.0466 \\ 0.0852 \\ -0.594 \\ 0.403 \\ 0.516 \end{bmatrix}$	$\boldsymbol{w}_4 = \begin{bmatrix} 0.4579 \\ 0.0466 \\ -0.0852 \\ -0.594 \\ -0.403 \\ 0.516 \end{bmatrix}$	$\boldsymbol{w}_{5,6} = \begin{bmatrix} 0 \pm 0.596i \\ 1 \pm 0 \\ 0 \pm 0.657i \\ 1.252 \pm 0i \\ 0 \mp 1.511i \\ 0.720 \mp 0i \end{bmatrix}$

used to generate a first-order approximation of the invariant 2-torus that produces quasi-periodic motion relative to a target spacecraft on the nearby L_2 halo orbit. Specifically, the normalized complex eigenvector is integrated via the linearized equations of relative motion and sampled at 1000 equally-distributed time instants. At each time step, the approximated invariant curve corresponding to $\varepsilon = 1$ km is calculated. The collection of these curves forms a first-order approximation of the associated 2-torus, displayed as a blue surface in the right subfigure of Fig. 5, along with the original invariant curve evaluated at apolune, plotted in black. Additional first-order approximations of invariant tori that exist near the periodic orbit may be generated by calculating the invariant curves at alternative values of ε.

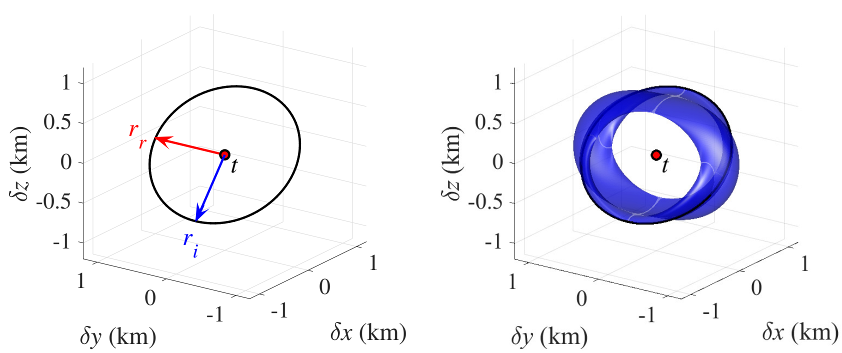

Fig. 5 Constructing a first-order approximation of an invariant 2-torus described by $\varepsilon = 1$ km in the configuration space relative to an Earth-Moon L_2 halo orbit: (left) projection of the first-order approximation of an invariant curve relative to apolune and (right) surface traced by the approximated invariant curve over one revolution of the periodic orbit

Stability analysis is used to identify a wider array of members of the Earth-Moon southern L_2 halo orbit family that admit oscillatory modes and, therefore, nearby quasi-periodic relative motion. The stability indices of periodic orbits within the computed segment of the Earth-Moon southern L_2 halo family are then plotted as a function of the orbit period in the center of Fig. 6. In addition, the stability indices of the four reference orbits highlighted in Fig. 4 are indicated using markers with a consistent color scheme. Analysis of this figure reveals that members within the computed segment of this family admit stability indices, s_1 and s_2, that lie between the critical values of -2 and 2. As a result, fixed points along these orbits produce a monodromy matrix with at least one set of complex eigenvalues that

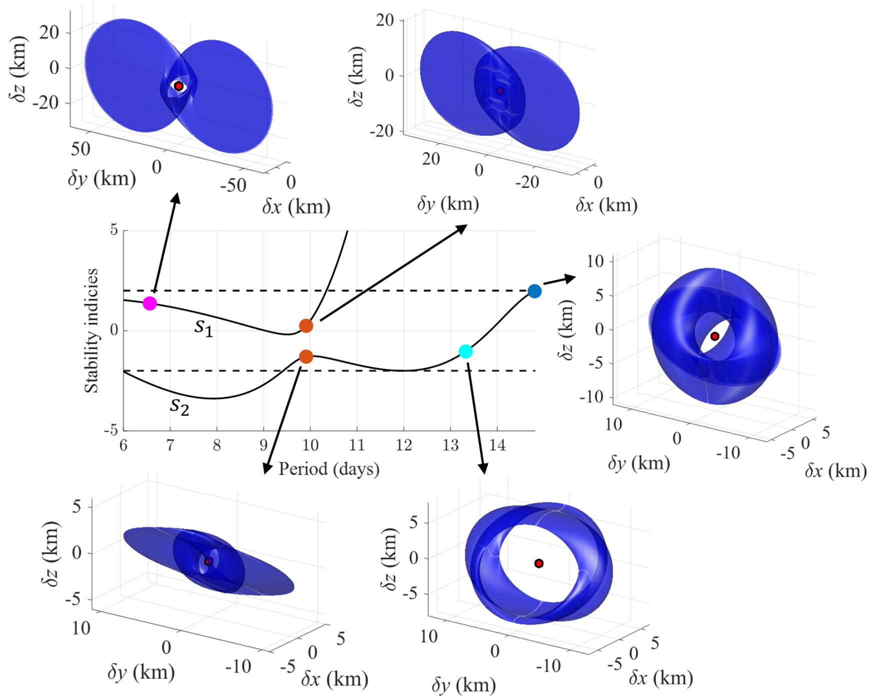

Fig. 6 Stability indices of periodic orbits across the Earth-Moon southern L_2 halo orbit family with selected first-order approximations of invariant 2-tori associated with the indicated oscillatory mode and ε = 10 km and displayed in relative position coordinates, measured from the target spacecraft

lie on the unit circle, indicating the presence of nearby quasi-periodic motion (Breakwell and Brown 1979; Howell 1984). For example, the oscillatory modes of the halo orbit near the bifurcation with the L_2 Lyapunov orbit family (blue), and the centrally located halo orbit (cyan) correspond to the s_2 index, while the oscillatory mode of the NRHO (magenta) corresponds to s_1. These orbits, represented by blue and cyan markers, also possess a stability index corresponding to a stable/unstable eigenvalue pair, equal to approximately $s_1 = 1137$ and $s_1 = 102$, respectively. The stable halo orbit (red), however, is located in a region of the L_2 halo orbit family where the orbits admit two pairs of oscillatory modes (Howell 1984). This stability analysis reveals that the presented local toroidal coordinate sets, defined based on first-order approximations of invariant 2-tori, may be used to study relative motion near a variety of members across the Earth-Moon southern L_2 halo orbit family.

At the boundaries of Fig. 6, the first-order approximations of invariant 2-tori associated with the highlighted members and generated by exciting the indicated oscillatory modes are plotted. Each torus is defined by ε = 10 km and visualized in the rotating frame. For each member of the L_2 southern halo orbit family, the complex eigenvector is normalized at apolune. The oscillatory modes corresponding to the s_1 index are characterized by large in-plane separation with maximum out-of-plane separation occurring at perilune. The tori generated by exciting the oscillatory modes corresponding to the s_2 index are characterized by ring-like structures with the largest components of separation in the $\hat{\boldsymbol{y}}$ direction at perilune.

This noticeable difference in the geometry of quasi-periodic relative motion produced by exciting each of the two oscillatory modes is also evident by comparing the two invariant 2-tori generated for the stable halo orbit that is highlighted in red. In fact, analysis of the boundaries of Fig. 6 reveals that the quasi-periodic relative motion near a single periodic orbit family may admit a variety of complex geometries. However, using the presented local toroidal coordinates, the trajectories that trace the illustrated tori are all described by the same quantities: $\varepsilon = 10$ km, value of θ between 0 and 2π rad, and $h = 0$ km. As a result, this straightforward and geometric coordinate description may facilitate the rapid generation and analysis of quasi-periodic relative paths in the CR3BP and, potentially, trajectory design for formations of spacecraft.

7.2 Error in first-order approximation of invariant tori

A numerical analysis is used to examine the error associated with a first-order approximation of quasi-periodic relative motion. This analysis is first demonstrated for motion along a single first-order approximation of an invariant torus near one L_2 southern halo orbit and then expanded to examine the error for a variety of tori near members that span the computed segment of the family, as plotted in Fig. 4. In each case, states along the following two types of distinct trajectories, expressed in toroidal coordinates and generated from the same initial condition that lie along one first-order approximation of an invariant curve, are compared: 1) trajectories generated using the nonlinear equations of motion and 2) sequences of states that are seeded from first-order invariant curves.

An invariant curve is calculated relative to apolune along the Earth-Moon L_2 southern halo orbit with a period of 13.3 days, as displayed in cyan in Fig 4, and used to generate the associated trajectories in each of the nonlinear and linearized models. First, 25 initial conditions are seeded from the first-order approximation of the invariant curve and expressed in geometric toroidal coordinates, using the complex eigenvector of the monodromy matrix computed and normalized at apolune. These initial conditions are described by the following values of the geometric toroidal coordinates: $\varepsilon = 10$ km and evenly distributed values of $\theta \in [0, 2\pi)$ rad, with values of h and the coordinates rates that are all initially set equal to zero to indicate motion that lies within the set $\boldsymbol{\varphi}$. Each initial condition that is initially defined in geometric toroidal coordinates is converted to a relative state vector formulated in the rotating frame. The 25 initial conditions are then propagated using the nonlinear equations of relative motion for two revolutions of the halo orbit, approximately 26.6 days.

The propagated trajectories are visualized relative to the halo orbit in Fig. 7. In the left subfigure of Fig. 7, the relative trajectories are plotted in black in the rotating frame. In the right subfigure of Fig. 7, the same trajectories are plotted in black in the nonsingular toroidal coordinate frame. Although these trajectories are projected onto the $\alpha\beta$ plane, small out-of-plane components exist. In addition, the first-order approximation of the invariant curve is plotted as a blue circle with a radius of 10 km in the toroidal coordinate frame along with the initial state of each trajectory, represented as blue markers. Visualization of the relative trajectories in the rotating frame reveals oscillatory motion about the halo orbit. However, visualization of the same relative trajectories in the toroidal frame supplies an additional level of insight as the departure of the trajectories from the linear approximation of the invariant curve is more clearly observed.

A single initial condition from the set displayed in Fig. 7 is used to generate a trajectory in both the nonlinear and linear relative motion models to further examine the use of geometric toroidal coordinates. Specifically, consider an initial condition located along an invariant

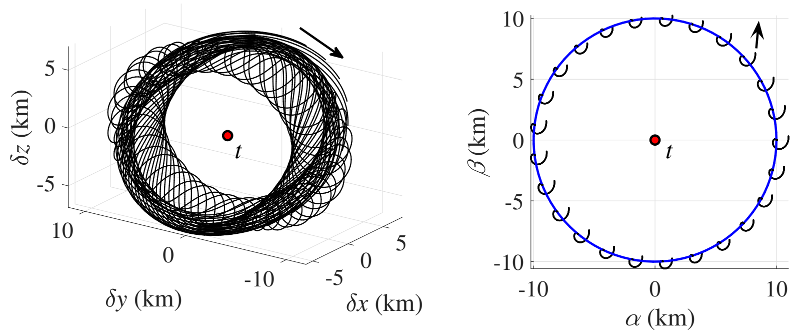

Fig. 7 Trajectories propagated in the CR3BP relative to an Earth-Moon L_2 southern halo orbit for two revolutions with initial conditions located along an invariant curve with $\varepsilon = 10$ km, defined relative to apolune, at evenly distributed values of θ. Trajectories are plotted relative to the periodic orbit in the: (left) rotating frame and (right) nonsingular toroidal coordinate frame

curve and described by $\varepsilon_0 = 10$ km and $\theta_0 = 0$ rad relative to apolune along the selected L_2 southern halo orbit; recall that the initial out-of-plane coordinate and all coordinate rates are set equal to zero. This initial condition possesses a relative Cartesian description in the rotating frame of $\boldsymbol{q}_0 = [0 \text{ km}, 10 \text{ km}, 0 \text{ km}, 0.0334 \text{ m/s}, 0 \text{ m/s}, 0.0192 \text{ m/s}]^T$. For the associated trajectories generated in the nonlinear and linear dynamical models, the geometric coordinates and coordinate rates are calculated at each integration time step and plotted in the subfigures of Fig. 8, represented in black and blue, respectively. The values of the geometric coordinates and coordinate rates along the trajectory in the linearized dynamical model are verified to remain constant to within 10^{-14} nondimensional units, similar to the tolerances used in numerical integration of the initial conditions in the linearized dynamical model.

Analysis of Fig. 8 reveals that, as expected in the CR3BP, the nonlinear trajectory gradually diverges from the linear approximation of the torus. Of course, relative motion associated with an initial condition within the first-order invariant set will eventually diverge from the vicinity of a periodic orbit with an unstable mode when propagated in the nonlinear model. Additionally, motion slightly perturbed from the center eigenspace, indicated by a nonzero value of h or nonzero toroidal coordinate rates, will excite other modes and produce similar behavior in the nonlinear model. Nevertheless, the local toroidal coordinates supply an intuitive description of nonlinear motion near a 2-torus relative to a periodic orbit.

This error analysis is expanded to analyze the divergence of nonlinear motion initialized along one first-order invariant curve for a wider variety of separations relative to members sampled across the computed segment of the Earth-Moon L_2 southern halo orbit family. Specifically, the geometric toroidal coordinates are used to define initial conditions relative to the state at apolune along members of the family for a range values of ε_0. This analysis supplies regions of validity for which the toroidal coordinates sufficiently predict initial conditions producing bounded motion in the nonlinear CR3BP. Values of ε_0 are selected within the range $\varepsilon_0 = [0, 100]$ km at an initial angle of $\theta_0 = 0$ rad along the first-order approximation of the associated invariant curve. Similar to the previous example, h_0 and the coordinate rates are all set to zero to ensure that the initial condition lies on an invariant curve relative to apolune. These initial conditions are then integrated from apolune for one revolution of the corresponding halo orbit using the nonlinear equations of relative motion. Errors in ε, θ, and h after one revolution, labeled as $\delta\varepsilon_f$, $\delta\theta_f$, and δh_f, respectively, are

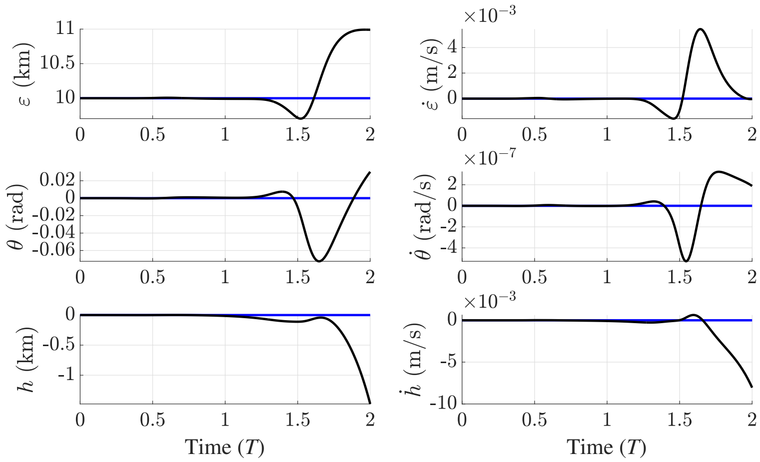

Fig. 8 Geometric local toroidal coordinates and coordinate rates evaluated along trajectories with the same initial condition, located along an invariant curve with $\varepsilon_0 = 10$ km and $\theta_0 = 0$ rad, and defined relative to apolune along an Earth-Moon L_2 southern halo orbit with a period of 13.3 days. Trajectories are propagated using the nonlinear CR3BP (black) and dynamical model linearized about the periodic orbit (blue)

defined as the difference between the final and initial values of the coordinates. The orders of magnitude of the errors are visualized using color and plotted as a function of both the period of the associated L_2 southern halo orbit on the horizontal axis and the initial value of ε, i.e., the size of the initial invariant curve, on the vertical axis in Figs. 9-11, respectively. Each figure includes two subfigures, corresponding to exciting one of the oscillatory modes associated with either s_1 or s_2 to generate quasi-periodic relative motion.

Although the errors generally evolve smoothly across the orbit family, two discontinuities are observed in Figs. 9-11. The first discontinuity is observed in the s_2 mode at the intersection of the s_2 stability index with -2, near an orbit possessing a period of approximately $T = 12$ days. Near this discontinuity, increased numerical sensitivity is observed in the computation of the approximated invariant curve due to the eigenvalues corresponding to the s_2 index possessing small imaginary components. Another discontinuity in the orbit family is observed in the s_1 mode near an orbit period of approximately $T = 9.6$ days. In this region of the halo orbit family, the geometry of the invariant curve at apolune corresponding to the s_1 index evolves such that the eccentricity of the ellipse instantaneously equals zero. When continuing the orbit family in either direction across this discontinuity, vectors aligned with the principal axes of the invariant curve switch, causing a discontinuity in the surfaces due to the normalization process of the complex eigenvector.

The differences between the nonlinear and linear trajectories, expressed in geometric toroidal coordinates, supply insight into the errors induced by the linear approximation of quasi-periodic relative motion across the orbit family. Analysis of Figs. 9-11 reveals that L_2 southern halo orbits near the bifurcation with the L_2 Lyapunov family, i.e., members that possess periods of approximately $T = 14.8$ days, exhibit larger differences between the nonlinear trajectories and the linear approximations after one period. In this region, the s_1 stability index possesses a large value, corresponding to unstable modes with eigenvalue magnitudes much greater than unity. In addition, the oscillatory motion corresponding to the

s_1 index reveals a region of increased errors near the range of halo orbits that possess a period of approximately 9 days. In this region, the invariant curve near apolune is nearly-rectilinear along the $\hat{\boldsymbol{y}}$ direction. Outside of this region, an error of less than 1 km is generally observed

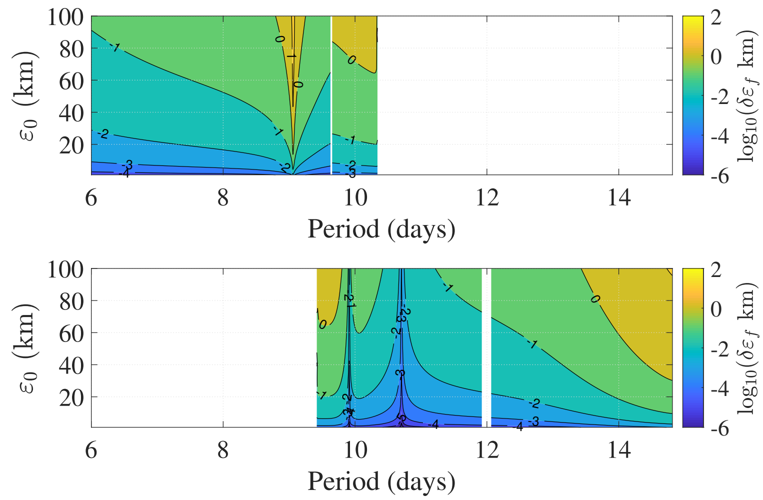

Fig. 9 Order of magnitude of error in ε after propagating selected trajectory for one revolution of a nearby L_2 southern halo orbit, represented as a function of the reference orbit period and initial value of ε corresponding to s_1 (top) and s_2 (bottom)

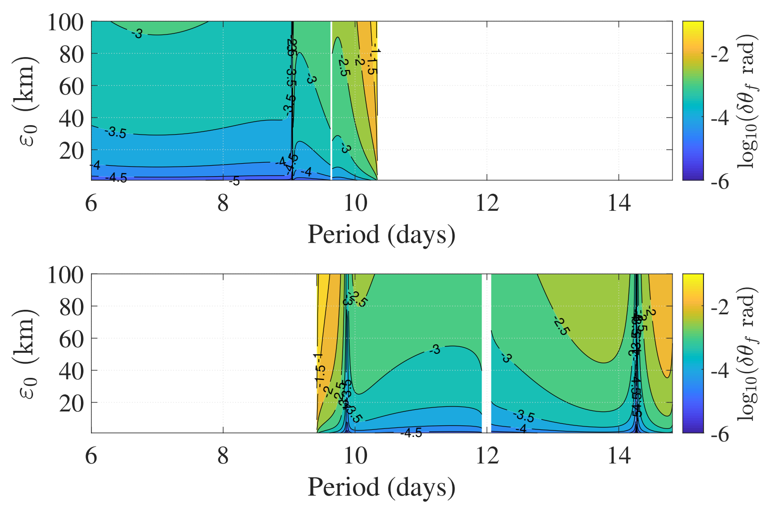

Fig. 10 Order of magnitude of error in θ after propagating selected trajectory for one revolution of a nearby L_2 southern halo orbit, represented as a function of the reference orbit period and initial value of ε corresponding to s_1 (top) and s_2 (bottom)

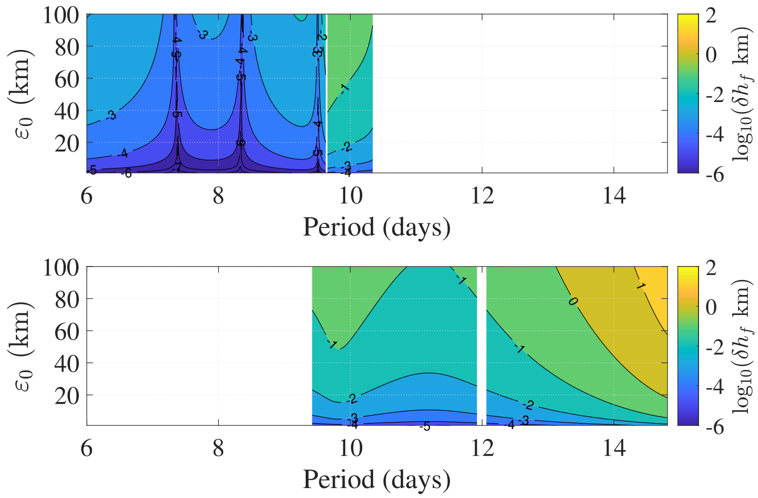

Fig. 11 Order of magnitude of error in h after propagating selected trajectory for one revolution of a nearby L_2 southern halo orbit, represented as a function of the reference orbit period and initial value of ε corresponding to s_1 (top) and s_2 (bottom)

in both ε and h, plotted in Figs. 9 and 10 respectively, for initial values of ε less than 50 km, i.e., the first-order torus with a maximum separation of 50 km from the periodic orbit at apolune. In Fig. 10, the differences in the initial and final angle are observed to be generally less than 5×10^{-3} rad for the same initial conditions.

The results depicted in Figs. 9-11 correspond to motion initialized relative to apolune along periodic orbits in the L_2 southern halo orbit family and at a single value of θ_0. Of course, modifying the reference fixed point, investigating different values of θ_0, or investigating values of ε greater than 100 km will alter the results. Nevertheless, the presented results supply preliminary insight into the deviation of these trajectories from the center eigenspace of the L_2 southern halo orbit family in the nonlinear CR3BP. In fact, for many members of this family, a first-order approximation of nearby quasi-periodic relative motion sufficiently predicts quasi-periodic relative motion in the nonlinear model for one revolution. Of course, nonlinear invariant tori that exist in the CR3BP are not exactly recovered in higher-fidelity models (Barden and Howell 1998b); rather, nearby trajectories may require control to maintain boundedness over specific time intervals.

7.3 Separation envelopes for oscillatory motion near the southern L_2 halo orbit family

This subsection examines the presented approximation for the separation envelope associated with quasi-periodic relative motion. First, the actual relative distances between a chaser and target spacecraft are calculated via the nonlinear equations of relative motion from initial conditions within the set $\boldsymbol{\varphi}$. These relative distances are then compared to the predicted magnitudes of the principal semi-axes over time, calculated using the method detailed in Section 6.

In this example, consider the 25 trajectories corresponding to quasi-periodic motion relative to the Earth-Moon L_2 southern halo orbit with a period of 13.3 days, as displayed in Fig. 7. The initial conditions of these 25 relative trajectories are seeded from the first-order approximation of the invariant curve with $\varepsilon = 10$ km relative to apolune. These states are then propagated forward in time for two periods using the nonlinear equations of relative motion. The separation distances between states along each of these trajectories and the nearby periodic orbit are measured isochronously and compared to the magnitude of the principal semi-axes of the first-order approximation of the invariant torus corresponding to $\varepsilon = 10$ km. The time histories of the separation distance for chaser spacecraft along each of these 25 trajectories are plotted in the top subfigure of Fig. 12 in black, along with the calculated magnitudes of the semi-major axis (red) and semi-minor axis (blue). In this figure, time is normalized by the period of the halo orbit, $T = 13.3$ days. Recall that the complex eigenvector associated with the oscillatory mode is also computed and normalized at apolune. The interpretation of ε as a result of this normalization is evident in Fig. 12: the maximum position separation at the initial condition, i.e., at apolune, is equal to $\varepsilon = 10$ km. Over the first revolution of the periodic orbit, the separation distances between a chaser spacecraft located along each of the nonlinear trajectories from a target spacecraft along the reference halo orbit predominantly remain within the maximum and minimum separation values predicted by r_a and r_b. In fact, the maximum error between the nonlinear motion and the estimated separation bounds over one orbit period is approximately 5 meters greater than r_a and approximately 8 meters less than r_b; both errors are significantly smaller than the separation distance. However, consistent with the prior error analysis, over the second revolution of the periodic orbit, gradual divergence of the nonlinear trajectories from the approximated range of motion is evident.

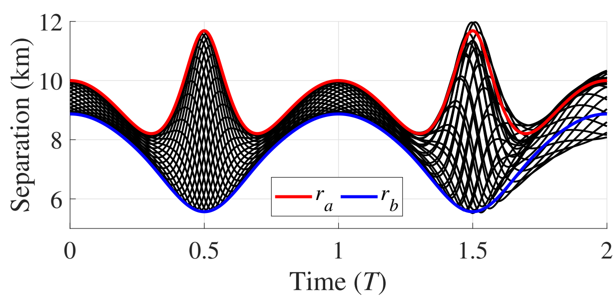

Fig. 12 Separation distance, measured from the 13.3 day Earth-Moon southern L_2 halo orbit, for the trajectories propagated using nonlinear equations of relative motion and displayed in Fig. 7. The time histories of the magnitudes of the principal semi-axes of the approximated invariant curve described by $\varepsilon = 10$ km are also plotted

The presented procedure is leveraged to conduct a broader examination of the separation envelopes associated with quasi-periodic relative motion near a range of members of the L_2 southern halo orbit family. For a discrete sample of Earth-Moon southern L_2 halo orbits displayed in Fig. 4, the magnitudes of the principal axes of the first-order approximation of a torus over time are computed using the process outlined in Section 6. The magnitudes of the principal semi-axes of the invariant curve are then plotted as a function of time after apolune, normalized by the period of the orbit, and the associated orbit, identified by orbit period.

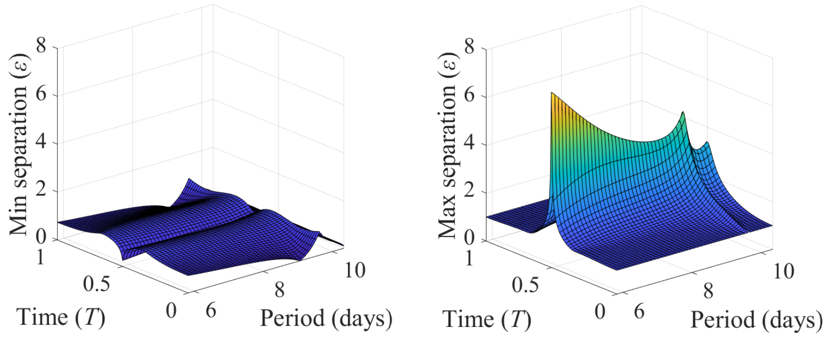

Fig. 13 Minimum (left) and maximum separation (right) of the first-order approximation of invariant tori exciting the s_1 index of associated members of the L_2 southern halo orbit family

The vertical axes are scaled to indicate the separation of the principal axes normalized by the value of ε of the torus. The result is a set of two-dimensional surfaces that bound the range of separations of approximated tori from the halo orbit family. The surfaces corresponding

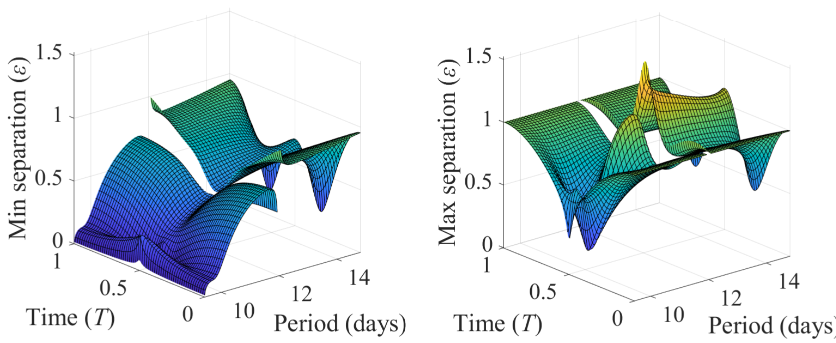

Fig. 14 Minimum (left) and maximum separation (right) of the first-order approximation of invariant tori exciting the s_2 index of associated members of the L_2 southern halo orbit family

to the s_1 and s_2 stability indices are visualized in Fig. 13 and Fig. 14, respectively. The color of the surfaces corresponds to the value along the vertical axis, for added visual clarity.

The surfaces of minimum and maximum separation reveal a complex variation in the deviation of oscillatory motion relative to periodic orbits across the L_2 southern halo orbit family. The two discontinuities observed in Figs. 9-10 are also visible in Figs. 13 and 14. Depending on the specific member of this family used to define the target spacecraft, the first-order approximation of an invariant torus may possess one or more local extrema in the maximum and minimum separation over time. Additionally, the differences between the maximum and minimum separation of a torus over time from the associated periodic orbit varies significantly across the family. For example, consider the motion excited by the oscillatory modes associated with s_2, represented in Fig. 14. For orbits with periods of approximately 10 days, natural quasi-periodic relative motion significantly contracts relative to the periodic orbit at a normalized time of 0.5, i.e., near perilune, indicated by simultaneously low values of r_a and r_b. In addition, for motion excited by the oscillatory modes associated with s_1 index, represented in Fig. 13, consider orbits in the near-rectilinear region of the family that possess a period of around 6 days. At perilune of these orbits, a simultaneously high r_a and low r_b is observed, indicating the torus admits a large variation in the separation distances from the periodic orbit.

To clearly visualize the variety of approximated separation extrema for a chaser spacecraft along a torus and measured relative to a target spacecraft along an L_2 southern halo orbit, their time histories are displayed for tori near the specific halo orbits highlighted in Fig. 6. These halo orbits are highlighted in the central plot of Fig. 15 and characterized via their stability indices and period. Then, the time histories of the separation extrema along tori near these selected members are plotted at the boundaries of Fig. 15 and normalized by torus size, ε: the red curves indicate the approximated maximum separation, while the blue curves display the approximated minimum separation. Rapid analysis of these characteristics across the orbit family may support the design of reference trajectories for spacecraft formations that seek to leverage naturally bounded motion relative to a periodic orbit but are subject to configuration constraints (Elliott and Bosanac 2022).

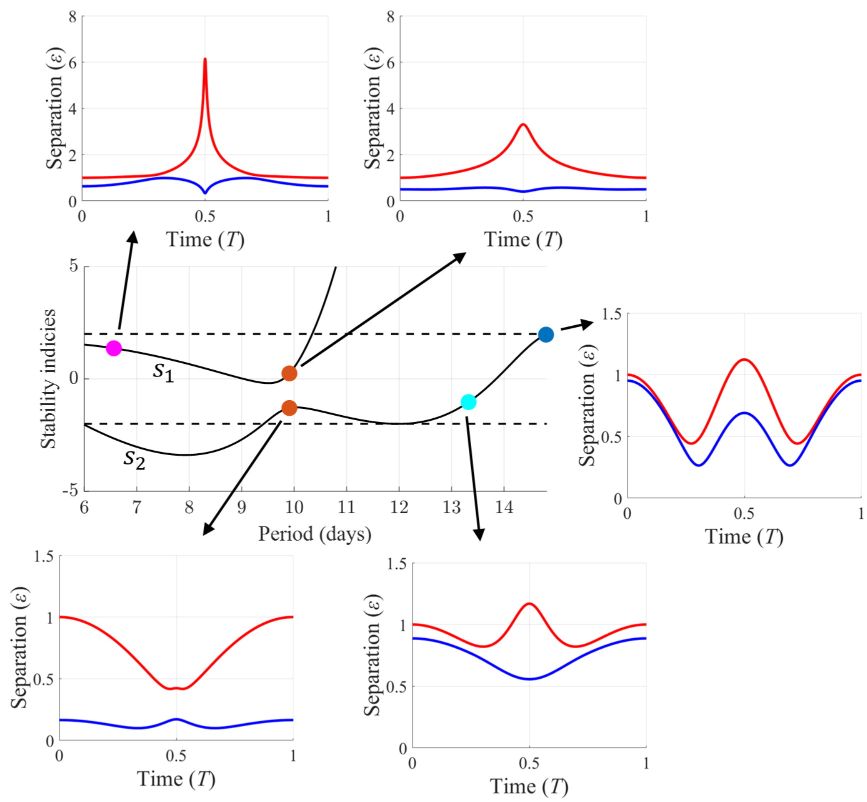

Fig. 15 Stability indices of periodic orbits across the Earth-Moon southern L_2 halo orbit family with the maximum (red) and minimum (blue) separation of selected first-order approximations of invariant 2-tori from the respective periodic orbits

8 Conclusions

This paper presents a family of local toroidal coordinate systems that are defined to support relative trajectory design and analysis near periodic orbits with oscillatory modes in the CR3BP. Specifically, the coordinate systems are defined using a first-order approximation of an invariant 2-torus as a reference. Furthermore, these coordinates are demonstrated analytically and numerically to supply a time-invariant description of motion on a first-order approximation of an invariant torus for equations of relative motion in the CR3BP linearized about a periodic orbit. Finally, a process for computing the instantaneous principal axes of the first-order approximation of an invariant curve associated with a single 2-torus is presented, leveraging integration of a singular value decomposition. This procedure enables a rapid prediction of the minimum and maximum possible separation between a chaser spacecraft located along an invariant torus relative to a target spacecraft along a nearby periodic orbit.

The toroidal coordinates and principal axes analysis are demonstrated in the context of quasi-periodic motion relative to a target spacecraft located along various members of the Earth-Moon L_2 southern halo orbit family. First, quasi-periodic relative motion initialized using geometric toroidal coordinates is studied across the L_2 southern halo orbit family using the linearized equations of relative motion. Then, the error between the nonlinear relative motion and the first-order approximation of quasi-periodic relative motion is analyzed across the L_2 southern halo orbit family and presented using the geometric coordinate set for various sizes of invariant curves defined relative to apolune. These results reveal a sufficiently small error, indicating that the first-order approximation of quasi-periodic relative motion within the toroidal coordinate systems is suitable for short-term analysis of motion at small separations from a periodic orbit. Finally, surfaces of the approximated minimum and maximum separation of a chaser spacecraft located along a torus and measured relative to a target spacecraft located along various members of the L_2 southern halo orbit are examined.

The geometric insight and slowly time-varying state description of spacecraft near quasi-periodic relative motion in multi-body systems motivates continued application and exploration of the local toroidal coordinates. For instance, the local toroidal coordinates may facilitate characterization of relative motion near other periodic orbit families in the Earth-Moon and Sun-Earth CR3BP that possess members with oscillatory modes, e.g., the L_1 and L_2 vertical orbits, distant retrograde orbits, or L_4 and L_5 short period orbits. A geometric interpretation of relative motion, achieved through the use of local toroidal coordinates, may also support formation geometry analyses and the formulation of targeting and control problems; both the focus of ongoing work by the authors (Elliott and Bosanac 2021a,b, 2022).

Acknowledgements This work was supported by a Graduate Assistance in Areas of National Need fellowship from the Smead Aerospace Engineering Sciences Department at the University of Colorado Boulder. An earlier version of this work was presented as AAS 20-620 at the AAS/AIAA Astrodynamics Specialist Virtual Conference in August 2020. The authors also wish to thank each of the reviewers for their feedback.

9 Declarations

Funding: This work was supported by a Graduate Assistance in Areas of National Need fellowship from the Smead Aerospace Engineering Sciences Department at the University of Colorado Boulder.

Conflict of interest: The authors declare that they have no conflict of interest.

Availability of data and material: No additional data or materials are provided.
Code availability: No additional codes are provided.

References

Alfriend, K., Vadali, S. R., Gurfil, P., How, J., and Breger, L. (2009). *Spacecraft Formation Flying: Dynamics, Control and Navigation*, volume 2, chapter 4: Nonlinear Models of Relative Dynamics, pages 59 – 82. Elsevier.

Bakhtiari, M., Daneshjou, K., and Abbasali, E. (2017). A new approach to derive a formation flying model in the presence of a perturbing body in inclined elliptical orbit: Relative hovering analysis. *Astrophysics and Space Science*, 362(2):36. https://doi.org/10.1007/s10509-016-2968-9.

Barden, B. T. and Howell, K. C. (1998a). Formation flying in the vicinity of libration point orbits. In *Advances in the Astronautical Sciences*, pages 969–988.

Barden, B. T. and Howell, K. C. (1998b). Fundamental motions near collinear libration points and their transitions. *J. Astronaut. Sci.*, 46(4):361–378. https://doi.org/10.1007/BF03546387.

Barden, B. T. and Howell, K. C. (1999). Dynamical issues associated with relative configurations of multiple spacecraft near the Sun-Earth/Moon L1 point. In *AAS/AIAA Astrodynamics Specialist Conference*.

Baresi, N. and Scheeres, D. J. (2017). Design of bounded relative trajectories in the Earth zonal problem. *J. Guid. Control Dyn.*, 40(12):3075–3087. https://doi.org/10.2514/1.G002603.

Baresi, N., Scheeres, D. J., and Schaub, H. (2016). Bounded relative orbits about asteroids for formation flying and applications. *Acta Astronaut.*, 123:364–375. https://doi.org/10.1016.

Belvin, W., Doggett, B. R., Watson, J., Dorsey, J. T., Warren, J., Jones, T. C., Komendera, E., Mann, T., and Bowman, L. (2016). In-space structural assembly: Applications and technology. In *AIAA Spacecraft Structures Conference*.

Bennett, T. and Schaub, H. (2016). Continuous-time modeling and control using nonsingular linearized relative-orbit elements. *J. Guid. Control Dyn.*, 39(12):2605–2614. https://doi.org/10.2514/1.G000366.

Breakwell, J. V. and Brown, J. V. (1979). The ‘halo’ family of 3-dimensional periodic orbits in the Earth-Moon restricted 3-body problem. *Celest. Mech.*, 20(4):389–404.

Burt, J. and Smith, B. (2012). Deep space climate observatory: The DSCOVR mission. In *IEEE Aerospace Conference*, Big Sky, MT. https://doi.org/10.1109/AERO.2012.6187025.

Calico, R. A. and Wiesel, W. E. (1984). Control of time-periodic systems. *J. Guid. Control Dyn.*, 7(6):671–676. https://doi.org/10.2514/3.19911.

Carter, T. E. (1998). State transition matrices for terminal rendezvous studies: Brief survey and new example. *J. Guid. Control Dyn.*, 21(1):148–155. https://doi.org/10.2514/2.4211.

Clohessy, W. H. and Wiltshire, R. S. (1960). Terminal guidance system for satellite rendezvous. *J. Aerosp. Sci.*, 27(9):653–658. https://doi.org/10.2514/8.8704.

Crusan, J. C., Smith, R. M., Craig, D. A., Caram, J. M., Guidi, J., Gates, M., Krezel, J. M., and Herrmann, N. B. (2018). Deep space gateway concept: Extending human presence into cislunar space. In *IEEE Aerospace Conference*, pages 1–10. IEEE.

Dunham, D. W. and Roberts, C. E. (2001). Stationkeeping Techniques for Libration-Point Satellites. *J. Astronaut. Sci.*, 49(1):127–144. https://doi.org/10.1007/BF03546340.

Elliott, I. and Bosanac, N. (2021a). Impulsive control of formations near invariant tori via local toroidal coordinates. In *32nd AAS/AIAA Astrodynamics Specialist Conference*.

Elliott, I. and Bosanac, N. (2021b). Spacecraft formation control near a periodic orbit using geometric relative coordinates. In *31st AAS/AIAA Spaceflight Mechanics Meeting*.

Elliott, I. and Bosanac, N. (2022). Characterizing natural relative motion of formations on invariant tori in multi-body systems. In *AIAA Scitech 2022 Forum*.

Farquhar, R. W. (1971). The utilization of halo orbits in advanced lunar operations. NASA Technical Note D-6365.

Farres, A., Webster, C., and Folta, D. (2018). High fidelity modeling of SRP and its effect on the relative motion of Starshade and WFIRST. In *Space Flight Mechanics Meeting*. https://doi.org/10.2514/6.2018-2227.

Ferrari, F. and Lavagna, M. (2018). Suitable configurations for triangular formation flying about collinear libration points under the circular and elliptic restricted three-body problems. *Acta Astronaut.*, 147:374–382. https://doi.org/10.1016/j.actaastro.2016.08.011.

Franzini, G. and Innocenti, M. (2019). Relative motion dynamics in the restricted three-body problem. *J. Spacecr. Rockets*, 56(5):1322–1337. https://doi.org/10.2514/1.A34390.

Gardner, J., Mather, J., Clampin, M., Doyon, R., Greenhouse, M., Hammel, H., Hutchings, J., Jakobsen, P., Lilly, S., Long, K., Lunine, J., Mccaughrean, M., Mountain, M., Nella, J., Rieke, G., Rieke, M., Rix, H.-W., Smith, E., Sonneborn, G., and Wright, G. (2009). The James Webb Space Telescope. *Space Science Reviews*, 123:485–606. https://doi.org/10.1007/s11214-006-8315-7.

Gill, E., D'Amico, S., and Montenbruck, O. (2007). Autonomous formation flying for the PRISMA mission. *J. Spacecr. Rockets*, 44(3):671–681. https://doi.org/10.2514/1.23015.

Gómez, G., Masdemont, J., and Simó, C. (1998). Quasihalo orbits associated with libration points. *JAS*, 46(2):135–176.

Gurfil, P. and Kasdin, N. (2004). Stability and control of spacecraft formation flying in trajectories of the restricted three-body problem. *Acta Astronaut.*, 54(6):433–453.

Hazeltine, R. D. and Meiss, J. D. (2003). *Plasma Confinement*, chapter 2: Review of Fundamentals, pages 21–36. Dover Publications.

Henry, D. B. and Scheeres, D. J. (2021). Expansion maps: Designing relative trajectories on quasi-periodic orbits. *J. Guid. Control Dyn.*, 44(3):457–468. https://doi.org/10.2514/1.G005492.

Héritier, A. and Howell, K. C. (2014). Dynamical Evolution of Natural Formations in Libration Point Orbits in a Multi-Body Regime. *Acta Astronaut.*, 102:332–340. DOI:10.1016/j.actaastro.2013.10.017.

Howell, K. C. (1984). Three-dimensional, periodic,'halo'orbits. *Celestial mechanics*, 32(1):53–71.

Howell, K. C. and Marchand, B. G. (2005). Natural and non-natural spacecraft formations near the L1 and L2 libration points in the Sun-Earth/Moon ephemeris system. *Dynamical Systems*, 20(1):149–173. https://doi.org/10.1080/1468936042000298224.

Hsiao, F. and Scheeres, D. (2002). The dynamics of formation flight about a stable trajectory. *J. Astronaut. Sci.*, 50(3):269–287. https://doi.org/10.1007/BF03546252.

Jorba, À. and Masdemont, J. (1999). Dynamics in the center manifold of the collinear points of the restricted three body problem. *Physica D: Nonlinear Phenomena*, 132(1):189–213. https://doi.org/10.1016/S0167-2789(99)00042-1.

Kasper, J., Lazio, J., Romero-Wolf, A., Lux, J., and Neilsen, T. (2019). The sun radio interferometer space experiment (sunrise) mission concept. In *2019 IEEE Aerospace Conference*, pages 1–11. https://doi.org/10.1109/AERO.2019.8742146.

Kolemen, E., Kasdin, N., and Gurfil, P. (2012). Multiple Poincaré sections method for finding the quasiperiodic orbits of the restricted three body problem. *Celest. Mech. Dyn. Astron.*, 112:47–74. https://doi.org/10.1007/s10569-011-9383-x.

Koon, W. S., Lo, M. W., Marsden, J. E., and Ross, S. D. (2006). *Dynamical Systems, the Three-Body Problem and Space Mission Design*. Marsden Books.

Le Moigne, J. (2018). Distributed spacecraft missions (DSM) technology development at NASA Goddard Space Flight Center. In *Institute of Electrical and Electronics Engineers International Geoscience and Remote Sensing Symposium*, pages 293–296. https://doi.org/10.1109/IGARSS.2018.8519065.

Lo, M. W. (1999). Satellite-constellation design. *Computing in Science and Engineering*, 1:58–67. https://doi.org/10.1109/5992.743623.

McCarthy, B. P. and Howell, K. C. (2021). Leveraging quasi-periodic orbits for trajectory design in cislunar space. *Astrodyn.*, 5(2):139–165. https://doi.org/10.1007/s42064-020-0094-5.

McCartin, B. J. (2013). A matrix analytic approach to conjugate diameters of an ellipse. *Appl. Mathematical Sciences*, 7(36):1797–1810.

Meiss, J. D. (2007). *Differential Dynamical Systems*, chapter 9: Hamiltonian Dynamics, pages 333–391.

Montenbruck, O., Kahle, R., D'Amico, S., and Ardaens, J.-S. (2008). Navigation and control of the TanDEM-X formation. *J. Astronaut. Sci.*, 56(3):341–357.

Noble, B. and Daniel, J. W. (1969). *Applied Linear Algebra*. Prentice-Hall.

Olikara, Z. P. and Scheeres, D. J. (2012). Numerical methods for computing quasi-periodic orbits and their stability in the restricted three-body problem. In *Advances in the Astronautical Sciences*, pages 911–930.

Roscoe, C. W., Vadali, S. R., and Alfriend, K. T. (2013). Third-body perturbation effects on satellite formations. *J. Astronaut. Sci.*, 60(3):408–433. https://doi.org/10.1007/s40295-015-0057-x.

Schaub, H. (2004). Relative orbit geometry through classical orbit element differences. *J. Guid. Control Dyn.*, 27(5):839–848. https://doi.org/10.2514/1.12595.

Schaub, H. and Junkins, J. (2014). *Analytical Mechanics of Space Systems*, chapter 14: Spacecraft Formation Flying, pages 709–792. AIAA Education Series. American Institute of Aeronautics and Astronautics, Incorporated. https://doi.org/10.2514/4.102400.

Scheeres, D. J., Hsiao, F.-Y., and Vinh, N. X. (2003). Stabilizing motion relative to an unstable orbit: Applications to spacecraft formation flight. *J. Guid. Control Dyn.*, 26(1):62–73. https://doi.org/10.2514/2.5015.

Schnizer, P., Fischer, E., and Schnizer, B. (2014). Cylindrical circular and elliptical, toroidal circular and elliptical multipoles fields, potentials and their measurement for accelerator magnets. arXiv:1410.8090.

Seeger, M., Hetzel, A., Dai, Z., Meissner, E., and Lawrence, N. D. (2017). Auto-differentiating linear algebra. arXiv:1710.08717.

Sengupta, P. and Vadali, S. R. (2007). Relative motion and the geometry of formations in keplerian elliptic orbits with arbitrary eccentricity. *J. Guid. Control Dyn.*, 30(4):953–964. https://doi.org/10.2514/1.25941.

Short, C. R., Blazevski, D., Howell, K. C., and Haller, G. (2015). Stretching in phase space and applications in general nonautonomous multi-body problems. *Celest. Mech. Dyn. Astron.*, 122:213–238. https://doi.org/10.1007/s10569-015-9617-4.

Simó, C., Gómez, G., Llibre, J., Martínez, R., and Rodríguez, J. (1987). On the optimal station keeping control of halo orbits. *Acta Astronaut.*, 15(6-7):391–397.

Spergel, D., Gehrels, N., Baltay, C., Bennett, D., Breckinridge, J., Donahue, M., Dressler, A., Gaudi, B., Greene, T., Guyon, O., et al. (2015). Wide-field infrarred survey telescope-astrophysics focused telescope assets. arXiv:1503.03757.

Sullivan, J., Grimberg, S., and D'Amico, S. (2017). Comprehensive survey and assessment of spacecraft relative motion dynamics models. *J. Guid. Control Dyn.*, 40(8):1837–1859. https://doi.org/10.2514/1.G002309.

Szebehely, V. (1967). *Theory of Orbits*. Academic Press.

Townsend, J. (2016). Differentiating the singular value decomposition. *Technical Report*. Accessed 29 April 2021.

Tschauner, J. and Hempel, P. (1965). Rendezvous zu einem in elliptischer bahn umlaufenden ziel. *Acta Astronaut.*, 11(2):104–109.

Vallado, D. A. and McClain, W. D. (2013). *Fundamentals of Astrodynamics and Applications*. Space Technology Library. Microcosm Press, 4th edition.

Wiesel, W. and Shelton, W. (1983). Modal control of an unstable periodic orbit. *J. Astronaut. Sci.*